ULTRASHORT PULSE SHAPING IN LINEAR RESONANT ABSORBERS

by

Gazi Habiba Akter

Submitted in partial fulfilment of the
Requirements for the degree of Master of Applied Science

at

Dalhousie University
Halifax, Nova Scotia
November 2011

DALHOUSIE UNIVERSITY

DEPARTMENT OF ELECTRICAL AND COMPUTER ENGINEERING

The undersigned hereby certify that they have read and recommend to the Faculty of Graduate Studies for acceptance a thesis entitled "ULTRASHORT PULSE SHAPING IN LINEAR RESONANT ABSORBERS" by Gazi Habiba Akter in partial fulfilment of the requirements for the degree of Master of Applied Science.

Dated: November 30, 2011

Supervisor: _____

Readers: _____

_____

DALHOUSIE UNIVERSITY

DATE: November 30, 2011

AUTHOR: Gazi Habiba Akter

TITLE: ULTRASHORT PULSE SHAPING IN LINEAR RESONANT ABSORBERS

DEPARTMENT OR SCHOOL: Department of Electrical and Computer Engineering

DEGREE: MASc. CONVOCATION: May YEAR: 2012

_____

Signature of Author

To my parents

Table of Contents

List of Tables

List of Figures

Abstract

Pulse shaping is the technique which controls the ultra-short pulse shape, and it became of great technological interest because of its potential applications in laser pulse compression, digital communications, microscopy etc. We demonstrate the idea of pulse-shaping technique and pulse propagation with low energy losses in a resonant linear absorbing medium. This thesis presents the results of a study of the propagation of Gaussian and hyperbolic secant ultrashort chirped and chirp-free pulses in homogeneously and inhomogeneously broadened resonant linear absorbers. Changes to the pulse shape and energy loss factor are presented as the pulse propagates in the absorber. The Fast Fourier method is used to numerically determine both the normalized intensity profile and the pulse spectrum.

Our results show that, for pulse durations shorter than the relaxation time, chirped pulses in absorbing media obey the area theorem, with their shape changing with the propagation distance. Simulation results of the spectra of chirped pulses clearly show the burning of a spectral 'hole' as the pulse propagates, with the pulse energy pushed away towards the wings. When compared to chirp-free pulses, chirped pulses reshape faster and develop wings in their tail due to initial phase modulation.

Simulation results of the energy loss factor show that chirped pulses propagating in resonant linear absorbers sustain less energy losses than do chirp-free pulses. A comparison of chirped secant and Gaussian pulses shows that secant pulses propagate with lower energy losses.

Analytic solutions are presented for long-distance asymptotic expressions of initial rms spectral bandwidth as well as for the attenuation factor of chirped Gaussian pulses. These analytical results are in agreement with numerical simulations. The comparison of energy losses of short chirped Gaussian pulses and long pulses of any profile in linear absorbers is also discussed in the thesis.

List of Abbreviations and Symbols Used

ω_0	Carrier frequency of the pulse
ϕ_t	Temporal phase
A	Amplitude of the pulse
C	Chirp parameter
m	Mass of the electron
e	Charge of the electron
x	Displacement of the electron
k_s	Spring constant
ϕ_ω	spectral phase
E	Electric field vector
H	Magnetic field vector
B	Magnetic flux
D	Electric displacement vector
μ_0	Vacuum permeability
ϵ_0	Permittivity of vacuum
P	Polarization vector
$\chi^{(1)}$	Susceptibility of the material
ω	Oscillating frequency
γ	Damping constant
Δ	Detuning of carrier frequency
n	Refractive index coefficient
$\mathcal{E}$	Slowly varying electric field envelope
$\mathcal{H}$	Slowly varying magnetic field envelopes
d	Individual dipole moment
β_0	Carrier propagation constant
β_1	Inverse group velocity
v_g	Group velocity

d_0	Characteristic dipole moment amplitude
σ	Atomic dipole moment
Ω	Quantum rabi frequency
T_0	Dipole relaxation time
T_{eff}	Total relaxation rate
k	Coupling constant
ω_{pe}	Plasma frequency
$\mathcal{R}$	Material response function
α	Inverse linear absorption length
β	Phase accumulator function
L_B	Beer's law absorption length
τ_p	Pulse width
ϕ_{tot}	Total instantaneous phase
T_Δ	Characteristics damping time
$g(\Delta)$	Detuning distribution function
ω_i	Instantaneous frequency
L_D	Dispersion length
T	Dimensionless time
Γ	Attenuation factor
Z	Dimensionless propagation distance
Δt	Pulse duration
$\Delta\omega$	Pulse spectral width

Acknowledgements

I am particularly thankful to my supervisor, Dr. Sergey Ponomarenko, for his proper and timely guidance, encouragement and support throughout the entire work. His expert guidance showed me the light at the end of every dark tunnel I encountered during this research.

I am indebted to the examining committee of this thesis - Dr. Zhizhang (David) Chen, and Dr. William J. Phillips. Their insightful comments have been really helpful not only to make necessary corrections of this thesis.

I would also like to extend my thanks to National Science and Engineering Research Council (NSERC), for funding this research.

I am also thankful to my colleagues (the fellow graduate students at the TOP laboratory of Dalhousie University), especially Franklin Che, Soodeh Haghgoo and Laleh Mokhtarpour for providing their scientific and technical insights. I am grateful to the ECE department at Dalhousie University for providing me necessary administrative supports.

I can not thank enough to my family members - my brothers, sisters and husband. It would be really difficult for me to complete this work without their immense support, encouragement and love.

Chapter 1

Introduction

1.1 Motivation and Objective

Ultrashort pulse generation has always been a preferred area of research in the field of laser pulse applications. Modern applications of ultra-short pulses provide new and advanced opportunities for commercial purposes. An ultrashort pulse can be defined as one with picosecond and femtosecond duration. This range of pulse can be generated from mode-locked lasers. Ultra-short optical pulses can be produced from longer pulses using optical pulse compression techniques [1]-[3]. Ultrashort pulse optical sources are of great technological interest due to their distinguishing features, which include 1) ultrashort duration 2) ultra-large spectral bandwidth 3) high peak power. Ultra-short optical pulses can be used in optical communication systems with long-distance and high bit rate.

To apply ultra-short pulses in suitable applications it is necessary to control their temporal shapes. This shaped pulse can be used in different optical applications. However, it is difficult to control ultrashort pulses from available laser sources. Therefore it is necessary to use a pulse shaper which produces more modified and sophisticated shapes of ultrashort pulses.

Pulse compressor [4] is another device which can control ultrashort pulse by controlling the spectral phase of the input pulse. Chirp is the most common component in pulse compression. In pulse compression, the initial width of a pulse can be changed by applying the proper amount of chirp, so that we generate short pulses from initially wide pulse optical sources. Another advantage is that, data transmission rates can be improved upto 40% by chirping [5].

In this study we introduce a new technique of pulse shaping, which can reshape the

incident profile of the input pulse. Pulse shaping is a new dimension of modern technologies that control the shape of ultrashort pulse, and also in many fields of modern optics where it is desirable to reshape the pulses from optical sources. Various pulse shaping techniques have been developed in the last few decades.

The objective of this thesis is to produce ultrashort shaped pulse with low energy loss.This thesis explores a new technique of pulse shaping by transmitting chirped pulse in linear resonant absorbers. To introduce the new technique of pulse shaping this thesis analyzes the behaviour of short chirped pulses in linear resonant absorbers, such as doped optical fibers or atomic vapors. Chirped pulse is chosen in this thesis for a number of reasons. First, a pulse considerably chirped by direct modulation has significant effects on optical communication systems. Secondly, data transmission quality can be improved by using a chirped Gaussian pulse. Thirdly, ultra-short chirped pulses can reduce the loss factor for sufficiently long propagation distances in coherent linear absorbers. This energy loss is comparably much less than using a long pulse. Fourthly, chirped pulses have shaping properties which open up interesting applications in the field of modern optics.

1.2 Pulse Shaping

Pulse shaping allows us to create modified and complex waveforms of pulses from optical sources of single pulse according to the user's specifications. Femtosecond pulses have extremely short duration, high peak power and large spectral bandwidth, so shaped femtosecond pulse is useful in different types of applications such as fiber communication, signal processing, laser spectroscopy, device characterization, solid state physics, etc. [6]. Optical devices have the ability to alter temporal shape of

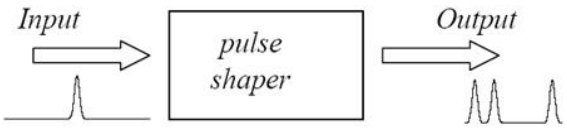

Figure 1.1: Pulse shaping of a band-limited pulse [7].

the pulse. Figure 1.1 shows an input pulse being converted into another shape by a

pulse-shaping method.

A particularly simple type of pulse shaping is pulse compression and/or stretching. Mainly based on the application pulse shapers are designed to compress or stretch a pulse and to generate a train of pulses. Dispersion of materials and optical devices is used to design the pulse shaper for compressing or stretching the pulse. Figure 1.2 shows the pulse shaper as a compressor and strecher.

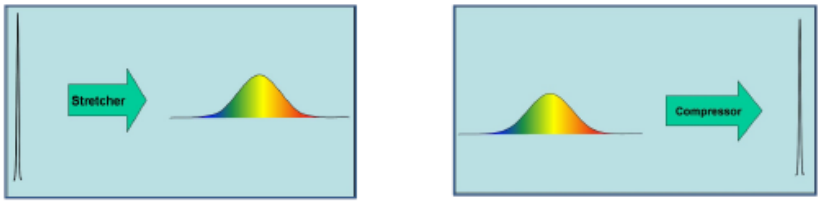

Figure 1.2: Pulse compressor and stretcher[8].

The basic concept of femtosecond pulse shaping can in most cases [1] be described by a linear time invariant filter, normally used to convert electrical signals from low to high frequencies. Linear filters are used to create shaped optical waves in picosecond and femtosecond time ranges. Figure 1.3 shows pulse shaping by a linear filter in time and frequency domains. In the time domain, the output pulse $E_{out}(t)$ is the convolution

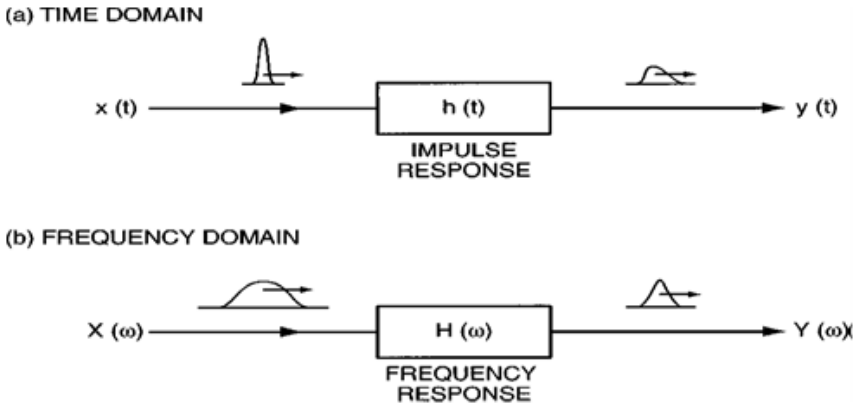

Figure 1.3: Time and frequency domain pulse shaping [9].

of input pulse $E_{in}(t)$ and $h(t)$. h(t) is the impulse response or modulation function

[1] In pulse compression technique phase of the pulse is modified by nonlinear effects.

that describes the modulation of phase and amplitude by the pulse shaping. This modulation can be described by

$$E_{out}(t) = E_{in}(t) \otimes h(t), \tag{1.1}$$

where $\otimes$ denotes a convolution. When a delta function is applied as an input pulse, the output is an impulse function. So in the case of sufficiently short input pulse, the perfect pulse shaping depends on a linear filter with a perfect impulse response. The response of the output, in the frequency domain, can be represented as

$$e_{out}(\omega) = e_{in}(\omega)H(\omega), \tag{1.2}$$

where $H(\omega)$ is the frequency response. In the case of delta function as an input pulse, the input spectrum $e_{in}(\omega)$ becomes unity, so that the output spectrum $e_{out}(\omega)$ is the frequency response function.

The two most common femtosecond pulse shaping techniques are 1) direct space-to-time pulse shaping and 2) Fourier transform pulse shaping. In direct space-to-time pulse shaping, the output of the pulse is directly dependent on the modulation function, while Fourier transform pulse shaping is implemented by Fourier transform, because a lens can do Fourier transforms in optics. A typical Fourier transform pulse shaping is shown in Figure 1.4.

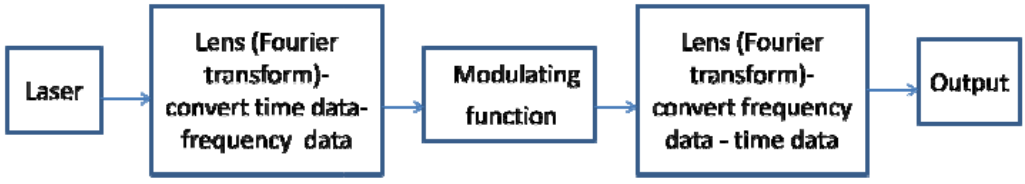

Figure 1.4: A typical Fourier transform pulse shaper

Direct space to time pulse shaper is commonly used when the required shape pulse is a pulse packet having discrete pulse series which are time separated. This pulse shaper is designed by direct mapping (no Fourier transform relationship) to desire temporal waveform. An example of such pulse shaping is parallel to serial conversion

[10].

Just over half a century ago, the generation of ultra-short pulses in picosecond and femtosecond time scales saw a breakthrough. In 1960, pulse compression techniques were implemented in chirped radar for the compression of picosecond pulses [11]-[16]. The pulse compressor mainly increases the spectral bandwidth of the initial pulse, after which it separates the frequency modulation by applying the proper dispersive delay line [17].

Optical pulse compression described by Diels and Ruldolph [18] occurs in two major steps. Pulse compression is a Fourier transform pulse shaping technique. Figure 1.5 shows the first step, where a phase modulation is applied on the band limited input pulse. This phase modulation can be obtained by self-phase modulation (SPM)

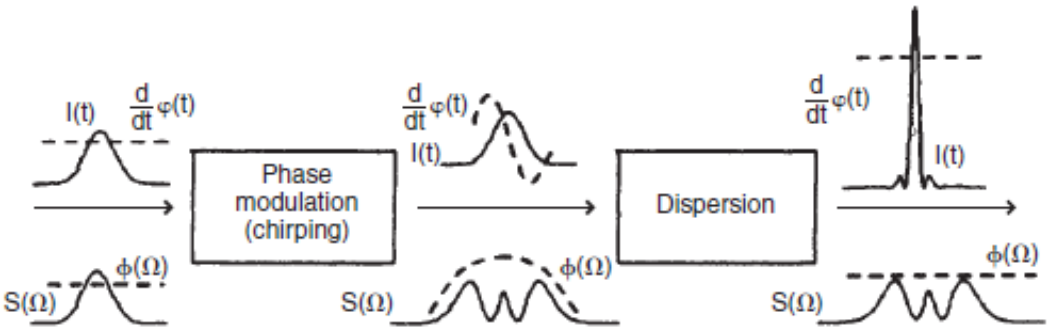

Figure 1.5: Optical pulse compression of a band-limited pulse [18].

which takes place in nonlinear media. The temporal intensity $|\mathcal{E}(t)|^2$ of the input pulse remains the same, but the phase $\phi(\Omega)$ of the pulse is modified by this phase modulation. In the time domain, the pulse becomes chirped and in the frequency domain, it is spectrally broadened.

The second step is dispersion (may be anomalous or normal) that can unchirp the chirped pulse generated in the first step. So this step appears as a Fourier transform of the first step. In the second step, dispersion modifies the phase of the pulse spectral field $\mathcal{E}(\Omega)$. The intensity of the spectral field $|\mathcal{E}(\Omega)|^2$ is not affected by dispersion. This step produces a band-limited output pulse from a spectrally broadened non

bandwidth-limited pulse. Since the pulse spectrum remains the same in the second step, the output pulse becomes shorter than the input pulse. For this reason the pulse compression process is also known as chirp compression.

Another example of a Fourier transform pulse shaping was demonstrated in the review article by Froehly in 1983 [19]. In his article, Froehly describes a Fourier transform pulse-shaping experiment in the picosecond range. In 1985, picosecond time scale pulses were shaped by using spatial filtering and grating pulse compression, as investigated by Heritage and Weiner [20].A non dispersive apparatus was used in 1988 to shape femtosecond pulses by initially using fixed masks and spatial filtering, with the shaped femtosecond pulses being manipulated by programmable spatial light modulators (SLM) [21, 22].

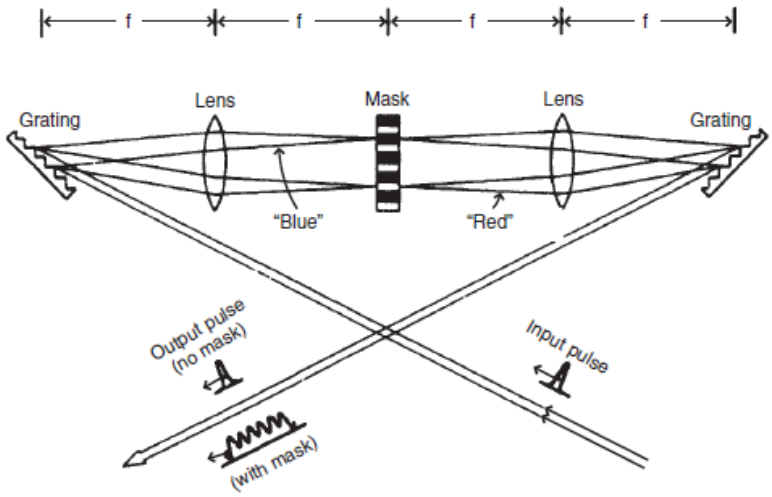

Figure 1.6: The typical setup for Fourier transform pulse shaping [18].

Figure 1.6 shows the basic Fourier transform pulse shaping layout, which has been modified from the first pulse-shaping apparatus mentioned by Froehly. The incident ultrashort (fms) pulses from a colliding pulse mode-locked (CPM) laser can be shaped by using a diffraction gratings pair, lenses, and a single pulse shaping mask. In the first part of the layout, the diffraction grating angularlydisperses the frequency components of the pulse, which are then transferred to the focal plane of the first lens in the rear side. The grating and lens are placed in such a way that the frequency components experience spatial separation. The first lens does a Fourier transform of the first grating output to convert the Fourier components to a spatial separation.

The amplitude and phase masks with a spatial pattern are set in the midway of the lens where the maximum spatial separation of the optical components occurs. Masks are spectrally filter the spatial dispersed frequency component. A shaped output is obtained after recombining all frequencies by a second lens and a second diffraction grating [9]. This setup of pulse shaping is also called the 4f pulse shaping arrangement. Dispersion for pulse stretching and compression is also possible without a mask by proper spacing of the grating-lens; this concept was introduced by Martinez [23] and now this idea is used in chirped pulse amplifiers (CPA). [24, 25].

1.3 Thesis Contributions

The major contribution of this thesis is that it has presented and demonstrated the idea of pulse shaping by transmitting prechirped pulses through coherent linear absorbing media. The behavior of ultrashort pulse propagation in linear resonant absorbers is studied in the presence of both homogeneous and inhomogeneous broadening. In this study, the classical area theorem has been derived and described with real and imaginary phase term for the first time to our knowledge. The pulse propagation equations are analytically described to evaluate the pulse spectrum, intensity and energy loss factor. Numerical simulations are also done using the fast Fourier method (FFT) [5, 26]. The simulation results show how ultrashort chirped pulses can modify their shape and dramatically reduce the energy loss when propagate through absorbers. The author of this research concentrated on developing the ideas and performing the analytical analysis and numerical simulations.

1.4 Thesis Outline

The thesis is organized as follows:

Chapter 2 describes the general theory of pulse propagation in linear optics with physical and mathematical explanations, including inhomogeneous and homogeneous line broadening of atoms. This is followed by a detailed discussion of the classical area theorem. The general solution of energy loss is introduced.

Chapter 3 presents the description of the propagation of chirped pulses and the effect of chirping in resonant linear optics.

In chapter 4, the simulation results for both chirped and unchirped pulses are presented. The numerical result and the analytical solution for a Gaussian pulse are also presented and compared.

Finally, Chapter 5 concludes the thesis work and provides some suggestions for future investigations.

Analytical solution of rms spectral bandwidth and attenuation factor for Gaussian pulse are presented in Appendices. Mathematica codes are also provided in the Appendices.

Chapter 2

Classical Theory of Light Propagation in Resonant Media

2.1 Introduction

In this chapter the classical theory of pulse propagation in optics will be summarized. Homogeneous and inhomogeneous line broadening and the classical area theorem will also be discussed in detail.

2.2 Classical Theory of Pulse Propagation in Optics

Pulse propagation in a linear resonant medium is a classic problem of optics [27]-[33]. In 1880, H. A. Lorentz proposed his classical theory, where the electron motion excited by an electromagnetic wave described by Newton's laws and the light fields obey Maxwell's equations. The Lorentz oscillator model presents the interaction of electric charges with the electromagnetic field. Most phenomena in optics (e.g., reflection and dispersion) can be described by the classical theory of the interaction of electric charges and radiation [34]. The electro-magnetic waves of the oscillating electric field will set the electron into harmonic motion, so that each material atom behaves as a simple harmonic oscillator and couples with the electromagnetic field through its dipole moment [28]. The damped harmonic oscillator accurately describes linear optical properties of atomic vapors, crystals, glasses and liquids.

The electron displacement is governed by the Lorentz equation in the form

$$m\frac{d^2x}{dt^2} = eE - k_s x - 2m\gamma\frac{dx}{dt}, \tag{2.1}$$

where m, e and x are the mass, charge and displacement of the electron, respectively, and k_s is the "spring" constant. The damping constant is γ. The motion of a dipole

can be expressed by

$$\frac{d^2x}{dt^2} + 2\gamma\frac{dx}{dt} + \omega_0^2 x = \frac{-eE}{m}. \tag{2.2}$$

Here the natural frequency is $\omega_0 = \sqrt{k_s/m}$. Free oscillations of electron around the nucleus are determined by natural frequency and damping rate is determined by the energy loss rate by electric dipole radiation.

Due to the electric field applied to a dielectric medium, electrons are separated from their original position by distance x and each atom has an individual dipole moment

$$d = ex. \tag{2.3}$$

Polarization field is determined by the individual dipole moment of each atom d and density of atoms N. So the polarization is

$$P = Nd = Nex. \tag{2.4}$$

The polarization field $\mathbf{P}$ is directly proportional to the electric field and is given by

$$\mathbf{P} = \epsilon_0 \chi^{(1)} \mathbf{E}, \tag{2.5}$$

where $\chi^{(1)}$ is the linear electric susceptibility and it is directly related with the medium.

Consider a plane electromagnetic wave with the electric field linearly polarized in the x-direction ($\mathbf{e_x}$) and propagating in z-direction, as

$$\mathbf{E} = \frac{1}{2}\mathbf{e}_x[E_0 e^{(kz-\omega t)} + c.c], \tag{2.6}$$

where E_0 is a complex amplitude of the wave, k is the propagation constant, ω is the wave frequency, and c.c is the complex conjugate.

The equation of motion for an electron oscillator driven by a monochromatic electromagnetic wave is

$$\frac{d^2x}{dt^2} + 2\gamma\frac{dx}{dt} + \omega_0^2 x = \frac{-eE_0}{2m} e^{-i\omega t} + c.c. \tag{2.7}$$

The driven solution of equation (2.7) is

$$x(t) = \frac{1}{2}[x_0 e^{-i\omega t} + c.c], \tag{2.8}$$

where

$$x_0 = \frac{-eE_0}{m(-\omega^2 + \omega_0^2 - 2i\omega\gamma)}. \tag{2.9}$$

The polarization field is

$$P(t) = -Nex(t) = \frac{Ne^2 E_0 e^{-i\omega t}}{2m(-\omega^2 + \omega_0^2 - 2i\omega\gamma)} + c.c. \tag{2.10}$$

The refractive index of the medium is related to polarization by

$$P(t) = \epsilon_0 \chi^{(1)} E(t) = \epsilon_0 (1 + n^2) E(t), \tag{2.11}$$

and solving for the refractive index gives

$$n^2 = \left(1 + \frac{Ne^2}{2m\epsilon_0}\left[\frac{1}{\omega_0^2 - \omega^2 - 2i\gamma\omega}\right]\right). \tag{2.12}$$

Here, the refractive index is complex $n = n_R + in_I$ and the real and imaginary parts are given by

$$n_R - 1 = \frac{Ne^2}{2m\epsilon_0}\left(\frac{\omega_0^2 - \omega^2}{(\omega_0^2 - \omega^2)^2 + \omega^2\gamma^2}\right). \tag{2.13}$$

$$n_I = \frac{Ne^2}{2m\epsilon_0}\left(\frac{\gamma\omega}{(\omega_0^2 - \omega^2)^2 + \omega^2\gamma^2}\right). \tag{2.14}$$

In Figure 2.1, the real and imaginary parts of the complex refractive index are known as the dispersion curve and absorption curve, respectively. In the real part, any region, where $dn/d\omega > 0$, is referred as normal dispersion, and for $dn/d\omega < 0$, is reffered as anomalous dispersion.

At normal dispersion, on the low frequency side, refractive index increases with increasing frequency and peaks when ω approaches to resonance frequency ω_0. At anomalous dispersion, at very near resonance (the ω close to ω_0) refractive index decreases rapidly to the minimum with increasing frequency and goes through zero at

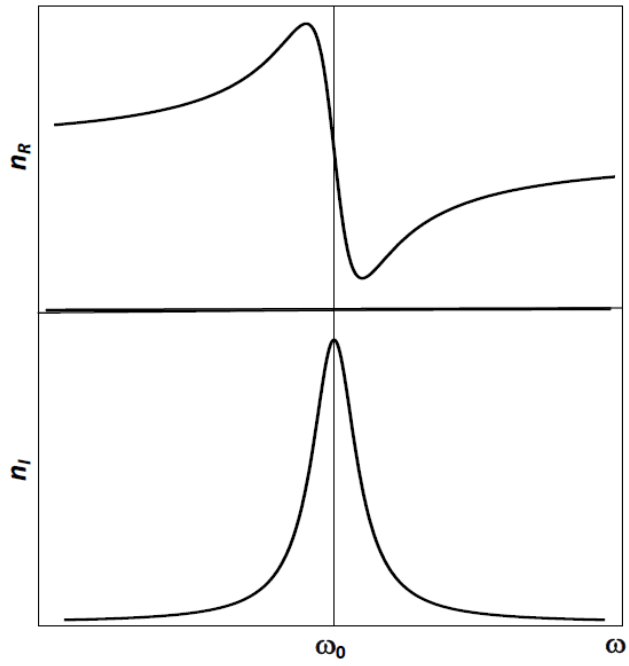

Figure 2.1: Typical plots of the real and imaginary parts of the refractive index.

ω_0. In this region, absorption is high and it occurs in a very narrow frequency region.

The imaginary part of the refractive index gradually increases and decreases with ω, and passes through the maximum. The center of the curve, the absorption peak, is located at ω_0 and the shape of imaginary part is a Lorentzian lineshape. The relationship between the two parts of the complex refractive index is known as the Kramers-Kronig relationship [35, 36].

2.3 Pulse Propagation Equation and Group Velocity Dispersion: Far From Optical Resonances

Consider pulse propagation in a linear dispersive medium, far away from any internal resonances. When a pulse propagates in such a medium, different frequency components are envolve with different speeds; for this reason the initial pulse profile will in general be distorted. When the group velocity of light is dependent on optical frequency or wavelength, the phenomenon is called group velocity dispersion (GVD).

Effects of group velocity dispersion of the medium far from any optical resonances are accounted for by the expanded equation of frequency dependent propagation constant β. Such expansion $\beta(\omega)$ in a Taylor series gives

$$\beta(\omega) = n(\omega)\frac{\omega}{c} = \beta_0 + \beta_1(\omega - \omega_0) + \frac{1}{2}\beta_2(\omega - \omega_0)^2 + ..., \tag{2.15}$$

where β_1 defines the inverse group velocity of the optical pulse envelope, $\beta_1 = \nu_g^{-1}$ and the second derivative term β_2 of the frequency dependent propagation constant describes pulse spreading. It is defined as

$$\beta_2 = \frac{d\beta_1}{d\omega} = \frac{d}{d\omega}\left(\frac{1}{\nu_g}\right) = -\frac{1}{\nu_g^2}\frac{d\nu_g}{d\omega}. \tag{2.16}$$

Another dispersion parameter commonly used in fiber optics to express dispersion in place of β_2, is defined as

$$D = \frac{d\beta_1}{d\lambda} = -\frac{2\pi c}{\lambda^2}\beta_2 = -\frac{\lambda}{c}\frac{d^2n}{d\lambda^2}. \tag{2.17}$$

For different signs of the GVD parameter β_2 or D, the effect of dispersion will be different on the optical pulse.

When the second derivative term $\beta_2 > 0$, the lower frequency components of the optical pulse go faster than their higher components; this is known as the normal dispersion regime. In this regime, the pulse creates positive chirps where the frequency increases with time. The dispersion is said to be anomalous when $\beta_2 < 0$, the revers happens and pulse creates negative chirps in this regime.

To quantitively explore pulse propagation in a nonmagnetic dielectric medium far away from optical resonances, we use Maxwell's equations in such a medium for the electric field $\mathbf{E}$ and magnetic field $\mathbf{H}$:

$$\nabla\cdot\mathbf{E} = 0. \tag{2.18}$$

$$\nabla\cdot\mathbf{H} = 0. \tag{2.19}$$

$$\nabla\times\mathbf{E} = -\mu_0\partial_t\mathbf{H}. \tag{2.20}$$

$$\nabla \times \mathbf{H} = \epsilon \partial_t \mathbf{E} + \partial_t \mathbf{P}, \tag{2.21}$$

where μ_0 is vacuum permeability, ϵ is a permittivity of the medium. From Maxwell's equations [37] it is easy to explain what happens when electromagnetic waves pass through a dielectric material. By taking the curl of Eq. (2.20)

$$\nabla \times (\nabla \times \mathbf{E}) = -\nabla \times (\mu_0 \partial_t \mathbf{H}) = -\mu_0 \partial_t (\nabla \times \mathbf{H}), \tag{2.22}$$

and a time derivative of Eq. (2.21) and then eliminating $\mathbf{H}$ we obtain

$$\nabla \times (\nabla \times \mathbf{E}) = \frac{1}{\epsilon_0 c^2} \partial_{tt}^2 \mathbf{P} + \frac{1}{c^2} \partial_{tt}^2 \mathbf{E} \tag{2.23}$$

where $c = 2.998 \times 10^8$ m/sec is the speed of light in vacuum and the relation $c = \frac{1}{\sqrt{\mu_0 \epsilon_0}}$.

After using the identity $\nabla \times (\nabla \times \mathbf{E}) = \nabla \cdot (\nabla \cdot \mathbf{E}) - \nabla^2 \mathbf{E}$ as well as Eq. (2.18), we obtain the general wave equation for the electric field $\mathbf{E}$ as

$$\nabla^2 \mathbf{E} - \frac{1}{c^2} \partial_{tt}^2 \mathbf{E} = \frac{1}{\epsilon_0 c^2} \partial_{tt}^2 \mathbf{P}. \tag{2.24}$$

Let us now consider a wave consisting of a slowly varying envelope $\mathcal{E}$ and a carrier plane wave such that

$$\mathbf{E} = \mathcal{E} e^{i(\beta_0 z - \omega_0 t)}, \tag{2.25}$$

where β_0 is a carrier propagation constant in the medium. On substituting from Eq. (2.25) into Eq. (2.24) we can arrive after minor algebra for the electric field envelope at the equation

$$\nabla^2 \mathcal{E} + \beta^2 \mathcal{E} = 0. \tag{2.26}$$

The slowly varying envelope approximation (SVEA) is considered for the condition where the envelope is separated from the fast varying carrier term. A slowly varying envelope approximation considerss that

$$\partial_z \mathcal{E} << \beta_0 \mathcal{E}. \tag{2.27}$$

Using Eq. (2.27) and (2.25) we arrive at

$$\nabla^2 \mathcal{E} \simeq 2i\beta_0 \partial_z \mathcal{E} - \beta_0^2 \mathcal{E}. \tag{2.28}$$

Next using Eq.(2.26), we arrive at the paraxial wave equation for the pulse envelope in the form

$$2i\beta_0\partial_z\mathcal{E} + [\beta^2(\omega) - \beta_0^2]\mathcal{E} = 0. \tag{2.29}$$

By using the perturbation approximation $\beta^2 - \beta_0^2 = 2\beta_0(\beta - \beta_0)$, Eq. (2.15) and Fourier transform properties, a paraxial wave equation for the temporal envelope is obtained in the form

$$2i(\partial_z\mathcal{E} + \beta_1\partial_t\mathcal{E}) - \beta_2\partial_{tt}^2\mathcal{E} = 0. \tag{2.30}$$

It is useful to employ a moving frame of reference by introducing the coordinate transformation:

$$\zeta = z; \qquad \tau = t - \beta_1 z. \tag{2.31}$$

After recalculating derivatives using the chain rules

$$\partial_t\mathcal{E} = \partial_\tau\mathcal{E}; \qquad \partial_{tt}^2\mathcal{E} = \partial_{\tau\tau}^2\mathcal{E}, \tag{2.32}$$

and

$$\partial_z\mathcal{E} = \partial_\zeta\mathcal{E} - \beta_1\partial_\tau\mathcal{E}, \tag{2.33}$$

we can arrive at the paraxial wave equation for the pulse propagation in linear dispersive media as

$$2i\partial_\zeta\mathcal{E} - \beta_2\partial_{\tau\tau}^2\mathcal{E} = 0. \tag{2.34}$$

Equation (2.34) describes pulse envelope propagation in linear dispersive media far from any optical resonances.

2.4 Pulse Propagation Near Optical Resonance

When an atom in an applied harmonic electric field oscillates very close to its natural frequency, this phenomenon is called the classical Rabi problem [28]. The equation of motion from sec. 2.2 can be applied to near resonant optical pulse propagation in

the positive z direction

$$\partial_t^2 x + 2\gamma\partial_t x + \omega_0^2 x = -eE/m, \tag{2.35}$$

The pulse field and atomic dipole moment can be represented as

$$E(z,t) = \frac{1}{2}[\mathcal{E}(z,t)e^{i(kz-\omega t)} + c.c]; \qquad ex(z,t) = \frac{1}{2}[d_0\sigma(z,t)e^{i(kz-\omega t)} + c.c]. \tag{2.36}$$

Here, $d_0 = ex_0$ is a characteristic dipole moment amplitude. Employing the SVEA

$$\partial_z\mathcal{E} << k\mathcal{E}, \qquad \partial_t\mathcal{E} << \omega\mathcal{E}, \tag{2.37}$$

$$\partial_t\sigma << \omega\sigma. \tag{2.38}$$

and using Eq. (2.35), (2.36) and (2.38), we can get the equation

$$-\omega^2\sigma - 2i\omega\partial_t\sigma - 2i\gamma\omega\sigma + \omega_0^2\sigma = -e\mathcal{E}/mx_0. \tag{2.39}$$

Near resonance

$$\omega_0^2 - \omega^2 \simeq 2\omega(\omega_0 - \omega) = 2\omega\Delta, \tag{2.40}$$

where $\Delta = \omega_0 - \omega$ is the detuning of the carrier wave frequency ω from the atomic resonance ω_0; near resonance the SVEA equation for atomic dipole envelope evolution is

$$\partial_t\sigma = -(\gamma + i\Delta)\sigma + i\Omega, \tag{2.41}$$

where the field envelope in frequency units is $\Omega = -e\mathcal{E}/2m\omega x_0$. Ω is also known as the Rabi frequency. Decomposing the dipole moment into in-phase U and quadrature V components as

$$\sigma(t,z) = U(t,z) - iV(t,z), \tag{2.42}$$

the equations for the in-phase and quadrature amplitudes then become

$$\partial_t U = -\gamma U + \Delta V, \tag{2.43}$$

and

$$\partial_t V = -\gamma V - \Delta U + \Omega, \tag{2.44}$$

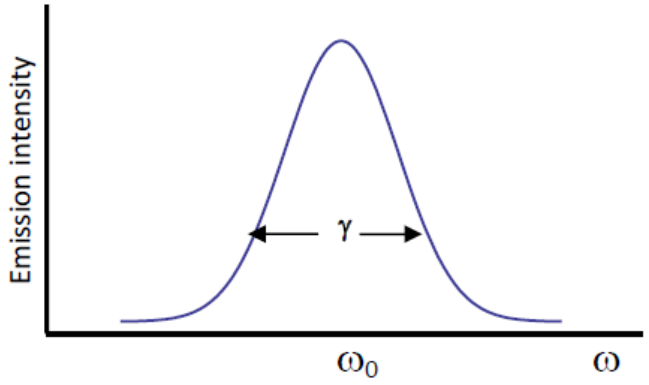

Figure 2.2: Lorentzian emission line with its homogeneous broadening.

In the absence of phase modulation, the real part U is referred to as the dispersive part and the imaginary part V is referred to as the absorptive part of σ. This is because U is coupled to the field only via the absorptive part and V is directly coupled to the electric field amplitude and affects the pulse envelope evoluation.

2.4.1 Homogeneous Line Broadening

Every material shows a large number of emission lines because of the oscillation of dipoles at different natural frequencies in real dielectrics. Due to the finite lifetime T_0 of every excited dipole moment, each emission line has a width in frequency, $1/T_0$. This spectral width is referred to as the width of homogeneous broadening because this width is the same for each dipole. Homogeneous broadening rate can be denoted by

$$\gamma = \frac{1}{T_0}. \tag{2.45}$$

Here, each dipole moment exponentially decays with time and the shape of the spectral line is Lorentzian. The homogeneous broadening of atomic dipoles is shown in Figure 2.2. It shows the individual Lorentzian emission line with its homogeneous width.

To derive the exponential decay law, consider decay of an atomic dipole moment introduced by a cw field in the past when the field is suddenly switched off, such that $\Omega(t) = \theta(-t)\Omega_0(z)$ where $\theta(t)$ is a unit step function. For $t > 0$, Ω becomes zero,

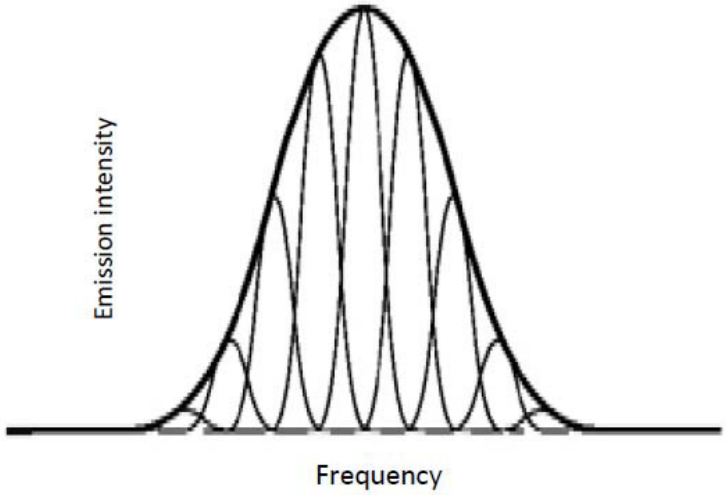

Figure 2.3: Inhomogeneous broadening of different dipoles in which dipoles are oscillated at different individual frequencies [38].

from Eq. (2.41) we get

$$\partial_t \sigma = -(\gamma + i\Delta)\sigma. \tag{2.46}$$

And the dipole moment envelope behaves as

$$\sigma(t, z) = \sigma(0, z)e^{-\gamma t}e^{i\Delta t}, \tag{2.47}$$

corresponding to a Lorentzian spectral line depicted in Figure 2.2.

2.4.2 Inhomogeneous Line Broadening

In gases and atomic vapours because of Doppler effect, atoms with different velocities suffer a Doppler shift in the frequency so that the atoms will "see" slightly different frequency of the carrier wave. In most cases, the real emission line is a combination of numerous Lorentzian lines with homogeneous width and a distinct center frequency. When the total line spread over a frequency range is compared with their broadened individual width, the overall line shape is known as being inhomogeneously broadened. Figure 2.3 shows inhomogeneous broadening, and the overall width of individual Lorentzian emission lines.

Inhomogeneous broadening is considered, as a large collection of identical atoms and fractional number of atoms where the resonance frequency is in between the value of ω_0 and $\omega_0 + d\omega_0$. So inhomogeneous broadening can be quantitively described by introducing a normalized inhomogeneous line shape function $g(\omega_0)$. The distribution function $g(\omega_0)$ is normalized to unity as

$$\int_0^\infty d\omega_0 g(\omega_0) = 1. \tag{2.48}$$

Using the dipole moment density near optical resonance we can write the polarization as

$$P(t,z) = \frac{1}{2}[Nd_0 \langle \sigma(z,t,\omega_0) \rangle e^{i(kz-\omega t)} + c.c]. \tag{2.49}$$

The averaging in the above equation is defined as

$$\langle \sigma(z,t,\omega_0) \rangle = \int_0^\infty d\omega_0 g(\omega_0) \sigma(z,t,\omega_0). \tag{2.50}$$

In reality, the distribution function is often peaked at some value of resonance frequency which is expressed by $\bar{\omega_0}$

$$g(\omega_0) \simeq g(\omega_0 - \bar{\omega_0}) = g(\Delta), \tag{2.51}$$

where $g(\Delta)$ is an inhomogeneous lineshape detuning function. The polarization can be rewritten as

$$P(t,z) = Nd_0 \int_\infty^\infty d\Delta g(\Delta) \sigma(t,z,\Delta). \tag{2.52}$$

By using Eq. (2.47) in free induction decay the polarization becomes

$$P(t,z) \propto Nd_0 e^{-t/T_0} e^{i\omega_0 t} \int_\infty^\infty d\Delta g(\Delta) e^{i\Delta t} + c.c. \tag{2.53}$$

Suppose the detuning distribution is Lorentzian, we can get

$$g(\Delta) = \frac{1}{(\Delta^2 + 1/T_\Delta^2)}, \tag{2.54}$$

where $1/T_\Delta$ characterizes the width of $g(\Delta)$. From Fourier transform table integration we can write

$$\int_\infty^\infty d\Delta g(\Delta) e^{i\Delta t} \propto e^{-t/T_\Delta} \tag{2.55}$$

If the detuning distribution function $g(\Delta)$ is Lorentzian and $t > 0$, the polarization is

$$P(t,z) \propto N d_0 e^{-t/T_{eff}} e^{i\omega_0 t} + c.c. \tag{2.56}$$

Here the total relaxation rate is

$$\frac{1}{T_{eff}} = \frac{1}{T_0} + \frac{1}{T_\Delta} \tag{2.57}$$

From sec. 2.4.1, we can say that the first term on the rhs of the above equation describes the homogeneous broadening and the second term describes inhomogeneous which occur in the spectral domain because of fluctuations of atomic detuning.

2.5 Pulse Propagation and Classical Area Theorem

With the plane wave propagation in the z-direction, the Doppler shifted frequency is

$$\omega' = \omega - k v_z. \tag{2.58}$$

In a moving reference frame the pulse field and atomic dipole moment distributions are

$$E(z,t) = \frac{1}{2}[\mathcal{E}(z,t)e^{i(kz-\omega' t)} + c.c]; \qquad ex(z,t) = \frac{1}{2}[d_0\sigma(z,t)e^{i(kz-\omega' t)} + c.c]. \tag{2.59}$$

From sec. 2.3 the electromagnetic field $\mathbf{E}$ of linear polarization obeys the wave equation in the form

$$\partial_{zz}^2 E - c^{-2}\partial_{tt}^2 E = \mu_0 \partial_{tt}^2 P, \tag{2.60}$$

and magnitude of polarization P is

$$P = -Ne\langle x \rangle . \tag{2.61}$$

Using Eq. (2.60), (2.59), (2.61) and SVEA (2.38), we can obtain the slowly-varying field envelope evolution in the form

$$\partial_z \Omega + c^{-1}\partial_t \Omega = i\kappa \langle \sigma \rangle , \tag{2.62}$$

where $\omega_{pe} = (Ne^2/\epsilon_0 m)^{1/2}$ is the electron plasma frequency and coupling constant is $\kappa = \omega_{pe}^2/4c$.

Again transforming to the moving reference frame using Eq. (2.31), we get the coupled Maxwell-Lorentz propagation equations

$$\partial_\zeta \Omega = i\kappa \langle \sigma \rangle , \tag{2.63}$$

and

$$\partial_\tau \sigma = -(\gamma + i\Delta)\sigma + i\Omega. \tag{2.64}$$

By using the Fourier transformation technique in Eq. (2.63) and (2.64), we obtain the field and dipole moment as

$$\tilde{\sigma}(\omega, \zeta) = \frac{i\tilde{\Omega}(\omega, \zeta)}{\gamma + i(\Delta - \omega)}. \tag{2.65}$$

and

$$\partial_\zeta \tilde{\Omega} = -k\mathcal{R}\tilde{\Omega}. \tag{2.66}$$

where $\mathcal{R}$ is the material response function defined as

$$\mathcal{R}(\omega) = \left\langle \frac{1}{\gamma + i(\Delta - \omega)} \right\rangle . \tag{2.67}$$

In the absence of inhomogeneous broadening

$$\mathcal{R}_{hom}(\omega) = \frac{1}{\gamma - i\omega} \tag{2.68}$$

After integrating Eq (2.66), we can write

$$\tilde{\Omega}(\omega, \zeta) = \tilde{\Omega}(\omega, 0) \exp\left[-k\mathcal{R}(\omega)\zeta\right], \tag{2.69}$$

The field envelope at any propagation distance can be written as

$$\mathcal{E}(\tau, \zeta) = \int_{-\infty}^{\infty} \tilde{\mathcal{E}}(\zeta, \omega) \exp(-i\omega\tau) d\omega = \int_{-\infty}^{\infty} d\omega \tilde{\mathcal{E}}(\omega) \exp\left[-i\omega\tau - k\mathcal{R}(\omega)\zeta\right], \tag{2.70}$$

where

$$\tilde{\mathcal{E}}(\omega) = \int_{-\infty}^{\infty} \frac{dt'}{2\pi} e^{i\omega t'} \mathcal{E}(t', 0). \tag{2.71}$$

From the combination of Eq. (2.70) and (2.71), we can obtain the field as

$$\mathcal{E}(t,z) = \int_{-\infty}^{\infty} \frac{dt'}{2\pi} \mathcal{E}(t',0) \int_{-\infty}^{\infty} d\omega e^{i\omega(t'-t)} \exp\left[i\omega z/c - k\mathcal{R}(\omega)z\right]. \tag{2.72}$$

The classical area theorem can be obtained from Eq. (2.72). The classical area $\mathcal{A}$ is defined as

$$\mathcal{A}(z) = \int_{-\infty}^{\infty} dt \mathcal{E}(t,z). \tag{2.73}$$

The integral representation of the delta function is

$$\delta(\omega) = \int_{-\infty}^{\infty} \frac{dt}{2\pi} e^{-i\omega t}. \tag{2.74}$$

Integrating Eq. (2.72) over time and using the integral representation of delta function, the area theorem is

$$\mathcal{A}(z) = \mathcal{A}_0 \int_{-\infty}^{\infty} d\omega \delta(\omega) \exp\left[i\omega z/c - k\mathcal{R}(\omega)z\right], \tag{2.75}$$

where $\mathcal{A}_0$ is the initial area under the pulse profile. Considering

$$f(\omega) = \exp\left[i\omega z/c - k\mathcal{R}(\omega)z\right], \tag{2.76}$$

and using the integral of delta function

$$\int_{-\infty}^{\infty} d\omega \delta(\omega) f(\omega) = f(0), \tag{2.77}$$

the resultant area theorem is

$$\mathcal{A}(z) = \mathcal{A}_0 \exp\left[-k\mathcal{R}(0)z\right]. \tag{2.78}$$

On substituting the material response function in Eq. (2.78) the area theorem can also be written in the form

$$\mathcal{A}(z) = \mathcal{A}_0 e^{-\alpha z/2} e^{i\beta z/2}, \tag{2.79}$$

where $\alpha = \left\langle \frac{2k\gamma}{\gamma^2+\Delta^2} \right\rangle$ is a characteristics attenuation decrement and $\beta = \left\langle \frac{2k\Delta}{\gamma^2+\Delta^2} \right\rangle$ is the phase accumulation factor. The area theorem states that regardless of the

initial pulse shape, in linear resonant absorbers the area under the pulse will decay exponentially.

If we follow the area theorem described by Allen and Eberly [28], it only includes the real attenuation decrement α. In our derivation of the area theorem we found that it also has imaginary phase term accumulation factor β. This imaginary term of the area theorem lets us generalize the area theorem to chirped pulses.

In the case of very long pulses where the characteristics pulse width is much longer than the homogeneous or inhomogeneous damping times,

$$T_p >> \max(T_0, T_\Delta), \tag{2.80}$$

the dipole moment decays fast to its equilibrium value. When this happens the rate of change of the dipole moment can be formally set to zero, i.e $\partial_\tau \sigma \simeq 0$. In this case, Eq. (2.64) becomes

$$\sigma \simeq \frac{i\Omega}{\gamma + i\Delta}. \tag{2.81}$$

Substituting Eq. (2.81) into Eq. (2.63), we obtain the pulse evolution as

$$\partial_\zeta \mathcal{E} = -\kappa \langle \frac{1}{\gamma + i\Delta} \rangle \mathcal{E}. \tag{2.82}$$

Now, the resulting envelope is

$$\mathcal{E}(t, z) = e^{-\alpha z/2} e^{i\beta z/2} \mathcal{E}_0(t - z/c). \tag{2.83}$$

where $\mathcal{E}_0(t)$ is a pulse profile in the source plane. Eq (2.83) is frequently designated as Beer's law in elementary optics treatment of absorbers. A long pulse propagates in absorbers with its initial form, and its amplitude decays exponentially with the propagation distance. This typical damping distance is known as Beer's absorption length $L_B = \alpha^{-1}$.

2.6 Energy Loss of Pulse

The pulse energy at any propagation distance within a resonant absorbing medium is determined by the square modulus of the field envelope,

$$W(z) \propto \int_{-\infty}^{\infty} dt \, |\mathcal{E}(t,z)|^2 \, . \tag{2.84}$$

By using Eq. (2.72) we can calculate the square modulus of the field envelope

$$|\mathcal{E}(t,z)|^2 = \int_{-\infty}^{\infty} d\omega' \int_{-\infty}^{\infty} d\omega \mathcal{E}(\omega,0)\mathcal{E}^*(\omega',0) e^{it(\omega'-\omega)} \exp[-\kappa z(\mathcal{R}(\omega)+\mathcal{R}^*(\omega'))]. \tag{2.85}$$

The energy at any propagation distance z is

$$W(z) = \int_{-\infty}^{\infty} d\omega' \int_{-\infty}^{\infty} \exp\left[\frac{-2z\alpha}{1+\omega^2 T_{eff}^2}\right] \mathcal{E}^*(\omega',0)\mathcal{E}(\omega,0) d\omega \int_{-\infty}^{\infty} dt e^{-it(\omega-\omega')}, \tag{2.86}$$

where we assumed a Lorentzian profile for inhomogeneous broadening. Again using integral representation of delta function we obtain

$$W(z) = \int_{-\infty}^{\infty} d\omega' \int_{-\infty}^{\infty} d\omega \mathcal{E}(\omega,0)\mathcal{E}^*(\omega',0) \exp\left[\frac{-2z\alpha}{1+\omega^2 T_{eff}^2}\right] 2\pi\delta(\omega-\omega'). \tag{2.87}$$

It follows from Eq. (2.87) that

$$W(z) = 2\pi \int_{-\infty}^{\infty} d\omega \, |\mathcal{E}(\omega,0)|^2 \exp\left[\frac{-2z\alpha}{1+\omega^2 T_{eff}^2}\right] . \tag{2.88}$$

For a numerical study it is convenient to transform to dimensionless variables, $Z = \alpha z$ and $\nu = \omega T_{eff}$. The energy attenuation factor of pulses is

$$\Gamma(Z) = W(Z)/W(0). \tag{2.89}$$

Now the energy at any propagation distance Z is expressed by

$$W(Z) = \int_{-\infty}^{\infty} d\nu \, |\mathcal{E}(\nu,0)|^2 \exp\left[-\frac{2Z}{(1+\nu^2)}\right] . \tag{2.90}$$

At propagation distance $Z = 0$, the energy is

$$W(0) = \int_{-\infty}^{\infty} d\nu \left|\mathcal{E}(\nu, 0)\right|^2 . \tag{2.91}$$

The resultant energy loss is in general given by the attenuation factor

$$\Gamma(Z) = \frac{\int_{-\infty}^{\infty} d\nu \left|\mathcal{E}(\nu, 0)\right|^2 \exp\left[-\frac{2Z}{(1+\nu^2)}\right]}{\int_{-\infty}^{\infty} d\nu \left|\mathcal{E}(\nu, 0)\right|^2}. \tag{2.92}$$

Chapter 3

Chirped Pulses in Resonance Linear Optics

3.1 Introduction

This chapter presents a general description of different shapes of chirped pulses often encountered in optics.

3.2 General Overview of Pulse and Chirp

The series of papers [5, 26, 39] by D. Marcus presented the Gaussian pulse distortion in a single mode optical fiber where the wavelength changes linearly (chirp) during propagation. A pulse whose instantaneous frequency varies with time is known as a chirped pulse.

Chirp appears in a pulse due to different phenomena. Chirp can arise in a pulse because of chromatic dispersion while it propagats in a transparent medium. Chirp can also result from diode lasers or amplifiers by direct modulation of lasers due to refractive index changes associated with the electron density.

The amount of chirp can be measured by the rate of change of instantaneous frequency (radians per second). When the instantaneous frequencies of any pulse increases or decreases with time, these are known as up-chirp and down chirp, respectively. Figure 3.1 shows an up-chirped pulse electric field where instantaneous frequency increases with time.

A chirped sinusoid wave has an instantaneous frequency that varies linearly with time. It can be represented by

$$\exp[i\omega_0 t] \rightarrow \exp i[\omega_0 t + C\frac{t^2}{2t_p^2}], \tag{3.1}$$

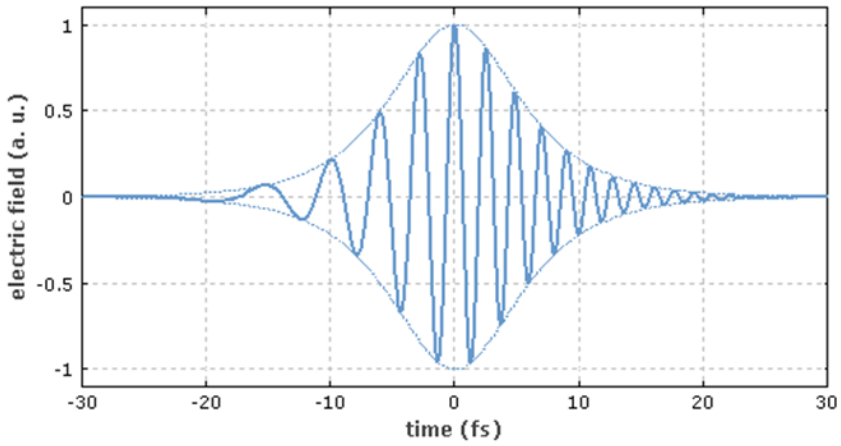

Figure 3.1: A pulse with a frequency "up-chirp" [40].

where ω_0 is the carrier frequency, t_p is a characteristic time related to the signal period and C is the (dimentionless) chirping parameter that represents the rate of change of the instantaneous frequency. The parameter C can be positive or negative, resulting in an increasing or decreasing instantaneous frequency.

Chirp can also be classified into linear and nonlinear chirp. Generally, the instantaneous frequency with a linear chirp changes linearly with time. The instantaneous frequency is

$$\omega(t) = \omega_0 + C\frac{t}{t_p^2}, \tag{3.2}$$

and the linearly chirped sinusoidal signal can be described as

$$v(t) = \sin\left[(\omega_0 + C\frac{t}{2t_p^2})t\right], \tag{3.3}$$

at unity amplitude, where ω_0 is frequency at $t = 0$.

Exponential chirp is a non-linear chirp, it is also known as geometric chirp [42, 43]. The instanteneous frequency of exponential chirp changes with time in a geometric relationship and the instantaneous frequency is

$$\omega(t) = \omega_0 C^{\frac{t}{t_p}}. \tag{3.4}$$

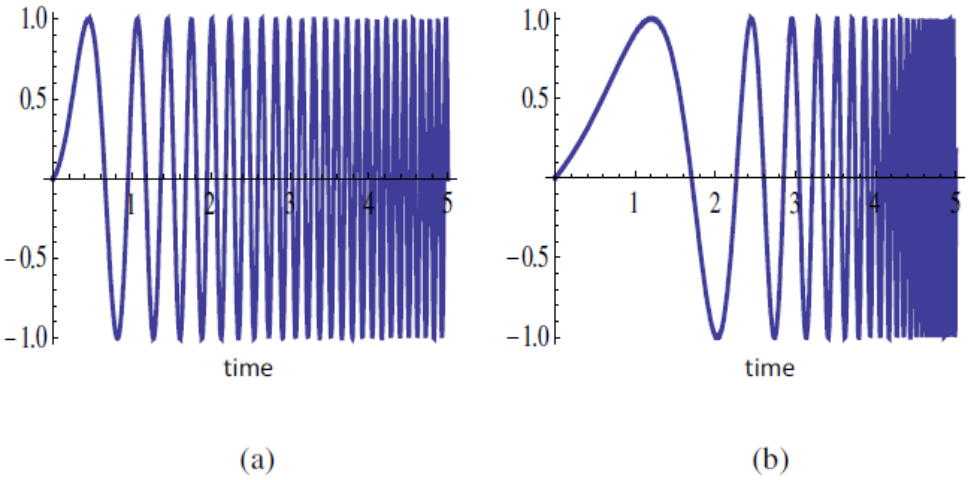

Figure 3.2: A pulse with (a) linear and (b) exponential chirp.

This type of chirped wave with unity amplitude is expressed as

$$v(t) = \sin(\omega_0(C^{\frac{t}{t_p}} - 1)/\ln C^{\frac{t}{t_p}}). \tag{3.5}$$

The chirp rate C is exponentially increasing in an exponentially chirped signal. Figure (3.2) (a) shows the linearly chirp waveform and (b) show the exponentially chirped wave-form where the instantaneous frequency varies linearly or exponentially with time, respectively.

One of the most important properties of a chirped pulse is that, it has a large bandwidth. Chirped pulses are used in a radar applications where a frequency swept (chirp) pulse is set into a linearly dispersive delay line [41] to improve the range resolution. Chirped pulses also have attractive properties of pulse shaping and they can modify the temporal profile of ultra-short pulses of a laser.

As a sufficient amount of chirp in a given input pulse can produce a short pulse, it is useful to create a short pulse from a wider pulse source. By this technique, ultra short pulses from a semiconductor laser can be further compressed. Broadening of optical pulses is induced by dispersion. Broadening and compression of chirped pulses depend on the same or opposite signs of dispersion and chirp parameters. For details see discussion in sec. 3.4.

3.3 Gaussian Envelope Function

In most cases, pulses emitted from a laser form a Gaussian-like shape, which is commonly used for investigation of pulse transmission in fiber optics [45]-[46]. The electric field of the Gaussian pulse can be written as

$$\mathcal{E}(t) \propto \exp[-\frac{t^2}{t_p^2}] \exp[i(\omega_0 t + C\frac{t^2}{2t_p^2})], \tag{3.6}$$

where t_p, ω_0 and C are the characteristic pulse width, carrier frequencye, and chirp parameter respectively. Here the Gaussian parameter of this pulse is $\Gamma = (1 - iC)/t_p^2$. If we consider the Gaussian pulse without chirp, the Gaussian parameter becomes $\Gamma = 1/t_p^2$. For $C > 0$, the instantaneous frequency rises linearly with time, from leading to the trailing edge (that's why, it is called up-chirp), for $C < 0$, the instantaneous frequency rises in opposite manner (it is called down-chirp).

The intensity $I(t)$ of the Gaussian pulse is given by

$$I(t) \propto |\mathcal{E}(t)|^2 = \exp[-2t^2/t_p^2] = \exp[-(4\ln 2)(t/\tau_p)^2]. \tag{3.7}$$

Here, τ_p is the Full Width at Half Maximum (FWHM) of the pulse which is related to t_p by the expression

$$\tau_p = t_p\sqrt{2\ln 2}. \tag{3.8}$$

3.3.1 Instantaneous Frequency

From Eq. (3.6) of the Gaussian pulse, the time-varying phase shift and the total instantaneous phase of the Gaussian pulse are represented respectively by [44]

$$\mathcal{E}(t) \propto \exp[i(\omega_0 t + C\frac{t^2}{2t_p^2})] = \exp[i\phi_{tot}(t)], \tag{3.9}$$

and

$$\phi_{tot}(t) = \omega_0 t + C\frac{t^2}{2t_p^2}. \tag{3.10}$$

The instantaneous frequency of Gaussian pulse $\omega_i(t)$ in unit of radians per second is expressed as

$$\omega_i(t) = \frac{d\phi_{tot}(t)}{dt}. \tag{3.11}$$

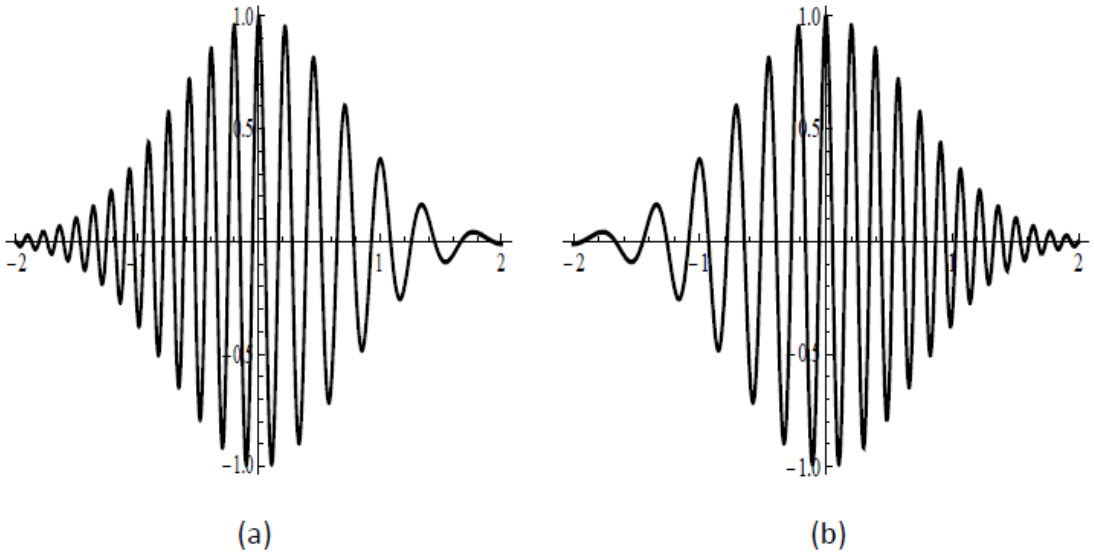

Figure 3.3: A (a) positively and (a) negatively chirped Gaussian signal pulse.

When a Gaussian pulse has a non-zero C and a linear time-varying instantaneous frequency, it is known as a chirped pulse. Figure 3.3 shows positively and negatively chirped Gaussian pulses with a linear time-varying instantaneous frequency. A pulse whose instantaneous frequency increases linearly from the leading to the trailing edge with time is called a positively chirped pulse. On the other hand, a negatively chirped pulse's instantaneous frequency decreases linearly with time.

3.3.2 Relationship Between Time and Frequency

Fourier transform of a Gaussian pulse can be obtained by

$$\mathcal{E}(t) = \frac{1}{2\pi}\int_{-\infty}^{\infty} \mathcal{E}(\omega)e^{-i\omega t}d\omega, \tag{3.12}$$

with the inverse given by

$$\mathcal{E}(\omega) = \int_{-\infty}^{\infty} \mathcal{E}(t) e^{i\omega t} dt. \tag{3.13}$$

The pulse width Δt can estimated using the r.m.s width concept

$$\Delta t = \sqrt{\langle t^2 \rangle - \langle t \rangle^2}, \tag{3.14}$$

where

$$\langle t^2 \rangle = \frac{\int_{-\infty}^{\infty} t^2 |\mathcal{E}(t)|^2 dt}{\int_{-\infty}^{\infty} |\mathcal{E}(t)|^2 dt}, \tag{3.15}$$

and $\langle t \rangle$ describes pulse center position

$$\langle t \rangle = \frac{\int_{-\infty}^{\infty} t |\mathcal{E}(t)|^2 dt}{\int_{-\infty}^{\infty} |\mathcal{E}(t)|^2 dt}. \tag{3.16}$$

Similarly for the spectral width

$$\Delta\omega = \sqrt{\langle \omega^2 \rangle - \langle \omega \rangle^2}, \tag{3.17}$$

where

$$\langle \omega \rangle = \frac{\int_{-\infty}^{\infty} \omega |\mathcal{E}(\omega)|^2 d\omega}{\int_{-\infty}^{\infty} |\mathcal{E}(\omega)|^2 d\omega}, \tag{3.18}$$

and

$$\langle \omega^2 \rangle = \frac{\int_{-\infty}^{\infty} \omega^2 |\mathcal{E}(\omega)|^2 d\omega}{\int_{-\infty}^{\infty} |\mathcal{E}(\omega)|^2 d\omega}. \tag{3.19}$$

The temporal and spectral widths are related by [47]

$$\Delta t \Delta\omega \geq 1/2. \tag{3.20}$$

It is clear from the above relationship that to produce a short pulse duration, need to use a large frequency range. When the product of the pulse duration and bandwidth is close to its minimum, the pulse is known as a Fourier-transform limited pulse. In experiments, it is easy to measure the half maximum quantities. Time frequency (Fourier inequality) product can be expressed by [47]

$$\Delta v \Delta t = K_A. \tag{3.21}$$

where Δv is the FWHM spectral width, Δt is half maximum time duration and K_A is a number depending on the profile of the pulse. Various symmetrical pulse shapes have values of K_A shown in table 3.1.

Table 3.1: K_A values for various pulse shapes [47].

Shape	**E(t)**	$\mathbf{K_A}$
Gaussian function	$\exp(-(t/t_0)^2/2)$	0.441
Exponential function	$\exp(-(t/t_0)/2)$	0.140
Hyperbolic secant	$1/\cosh(t/t_0)$	0.315
Lorentzian function	$[1+(t/t_0)^2]^-1$	0.142

3.4 Chirped Gaussian Pulse

The propagation and broadening of a chirped Gaussian pulse in a linear dispersive medium far from optical resonaces is reviewed in this section. Consider a linearly chirped Gaussian pulse with the initial pulse profile

$$\mathcal{E}(0,t) \propto \exp\left(-\frac{(1+iC)t^2}{2t_p^2}\right) \tag{3.22}$$

The amplitude $\mathcal{E}(z,t)$ of chirped Gaussian pulse at any propagation distance can also be evaluated analytically to give

$$\mathcal{E}(z,t) = \frac{1}{2\pi}\int_{-\infty}^{\infty} \tilde{\mathcal{E}}(z,\omega)\exp(-i\omega t)d\omega, \tag{3.23}$$

where the Fourier amplitude can be determined by

$$\mathcal{E}(z,\omega) = \int_{-\infty}^{\infty} \tilde{\mathcal{E}}(z,t)\exp(i\omega t)dt \tag{3.24}$$

Using paraxial wave Eq. (2.34) the pulse envelope at any distance z,

$$2i\partial_z\mathcal{E} - \beta_2\partial_{tt}^2\mathcal{E} = 0. \tag{3.25}$$

Using Eq. (3.23) the pulse dispersion equation can be written as

$$i\partial_t\tilde{\mathcal{E}} = -\frac{1}{2}\beta_2\omega^2\tilde{\mathcal{E}}. \tag{3.26}$$

A simple solution for the Fourier transform is

$$\tilde{\mathcal{E}}(z,\omega) = \tilde{\mathcal{E}}(0,\omega)\exp\left(\frac{i}{2}\beta_2\omega^2 z\right). \tag{3.27}$$

For chirped Gaussian pulse spectrum at $z = 0$ is

$$\tilde{\mathcal{E}}(0,\omega) = \int_{\infty}^{\infty}\tilde{\mathcal{E}}(0,t)\exp(i\omega t)dt \propto \frac{t_p}{\sqrt{2\pi(1+iC)}}\exp\left[-\frac{\omega^2 t_p^2}{2(1+iC)}\right] \tag{3.28}$$

The pulse envelope at any propagation distance z is

$$\mathcal{E}(z,t) \propto \frac{t_p}{[t_p^2 - i\beta_2 z(1+iC)]^{1/2}}\exp\left[-\frac{(1+iC)t^2}{2[t_p^2 - i\beta_2 z(1+iC)]}\right]. \tag{3.29}$$

The chirped Gaussian pulse retains its Gaussian shape during propagation. The pulse width at propagation distance z is

$$\Delta t(z) = t_p\left[\left(1+\frac{\beta_2 zC}{t_p^2}\right)^2 + \frac{\beta_2^2 z^2}{t_p^4}\right]^{1/2}. \tag{3.30}$$

Figure 3.4 shows that in chirped Gaussian pulses the broadening factor depends on

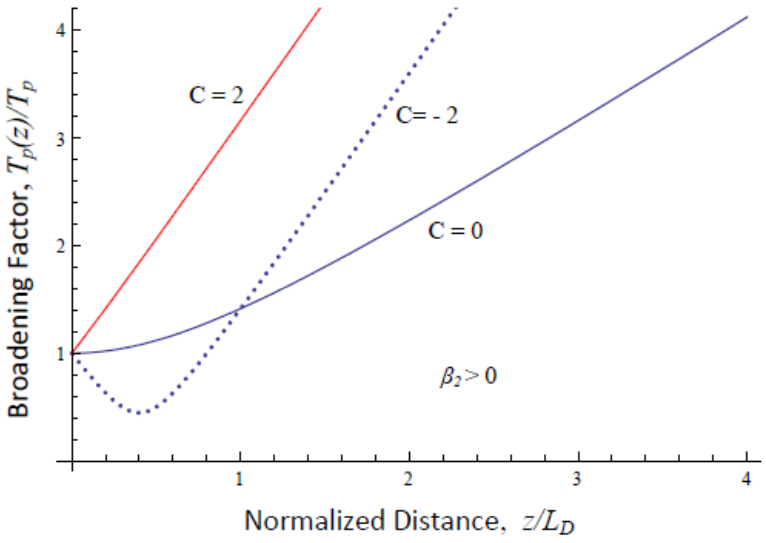

Figure 3.4: Broadening factor as a function of normalized distance z/L_D. For $\beta_2 < 0$ the same curve is obtained if the sign of the chirp parameter is reserved.

the relative signs of β_2 and C. If $\beta_2 C > 0$, the Gaussian chirped pulse is broadened faster than an unchirped Gaussian pulse at the same normalized distance z/L_D. When the pulse is initially chirped and $\beta_2 C < 0$ the chirp i induced by dispersion in the opposite direction from initial chirp. As a result the broadening factor goes through an initial compression stage. The minimum pulse width occurs when the two chirps are cancelled out. When the propagation distance is increased further, the pulse width will increase again.

3.5 Hyperbolic Secant Pulse

Mode-locked lasers often emit pulses having a temporal shape of hyperbolic secant (sech). The incident field of the hyperbolic secant pulse can be expressed by

$$\mathcal{E}(0,t) = \text{sech}\left(\frac{t}{t_p}\right). \tag{3.31}$$

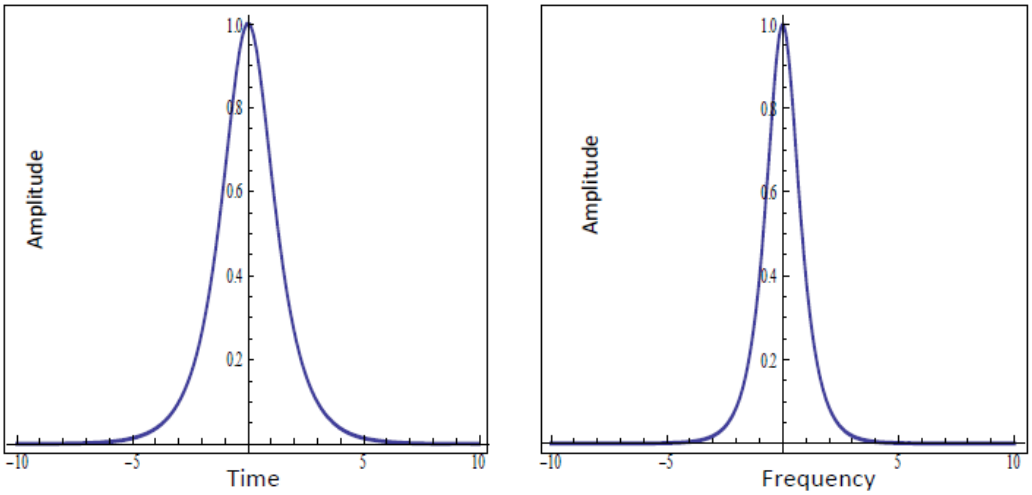

Figure 3.5: Temporal shape and pulse spectrum of a hyperbolic secant pulse at $t_p = 1$.

The full width at half-maximum of a secant pulse is

$$t_{FWHM} = 2\ln(1+\sqrt{2})t_p \approx 1.763 t_p. \tag{3.32}$$

The incident field of the chirped Hyperbolic secant pulse can be expressed by[48]

$$\mathcal{E}(0,t) = \operatorname{sech}\left(\frac{t}{t_p}\right) \exp\left(-\frac{iCt^2}{2t_p^2}\right). \tag{3.33}$$

Figure 3.5 shows the pulse profile and spectrum of a hyperbolic secant pulse without chirp.

Chapter 4

Ultrashort Pulse Shaping in Resonant Absorbers

4.1 Introduction

Numerical analysis of different shapes of chirped pulses propagating in coherent resonant absorbers is described in this chapter. Mathematical modeling and simulations were performed using the Mathematica software package.

4.2 Propagation of Chirped Pulses and Anomalous Losses

In this Chapter, we examine propagation of chirped ultrashort pulses of different shapes, which are often encountered in applications, in resonant linear absorbers. Recall that from Sec. 2.5 Eq. (2.70) the pulse envelope at any propagation distance inside the medium is given by

$$\mathcal{E}(t,z) = \int_{-\infty}^{\infty} d\omega\, \tilde{\mathcal{E}}(\omega)\, \exp[-i\omega(t - z/c) - \kappa\mathcal{R}(\omega)z], \tag{4.1}$$

where we introduced the spectral amplitude of the incident pulses viz.,

$$\tilde{\mathcal{E}}(\omega) = \int_{-\infty}^{\infty} \frac{dt'}{2\pi}\, \mathcal{E}(t',0)\, e^{i\omega t'}, \tag{4.2}$$

and the spectral response function $\mathcal{R}(\omega)$ of the medium is given by

$$\mathcal{R}(\omega) = \int_{-\infty}^{\infty} d\Delta\, \frac{g(\Delta)}{\gamma + i(\Delta - \omega)}. \tag{4.3}$$

In this Chapter, we consider a Lorentzian profile for the inhomogeneous broadening,

$$g(\Delta) = \frac{1}{\pi}\, \frac{1/T_\Delta}{(\Delta^2 + 1/T_\Delta^2)}. \tag{4.4}$$

It follows from Eqs. (4.3) and (4.4) that

$$\mathcal{R}(\omega) = \frac{1}{\gamma_{eff} + i(\Delta - \omega)}, \tag{4.5}$$

where the effective damping rate is given by the expression

$$\gamma_{eff} = \frac{1}{T_0} + \frac{1}{T_\Delta}. \tag{4.6}$$

$1/T_0$ describes the damping rate of homogeneously broadened atoms, and the characteristics damping time T_Δ and detuning distribution $g(\Delta)$ is associated with inhomogemeous broadening. So that Eq. (4.5) is satisfied by both homogeneous and inhomogeneous broadened atoms.

4.2.1 Chirped Gaussian Pulses

We first explore the behavior of a Gaussian pulse because it models well the output of most lasers [48]. The field profile of a chirped Gaussian pulse is given by the expression

$$\mathcal{E}(t, 0) \propto \exp\left[-\frac{(1 + iC)t^2}{2t_p^2}\right], \tag{4.7}$$

where t_p is a characteristic pulse width and C is a pulse chirp parameter. The spectral amplitude of the pulse is then given by

$$\tilde{\mathcal{E}}(\omega) \propto \exp\left[-\frac{\omega^2 t_p^2}{1 + C^2}\right] \exp\left[\frac{iC\omega^2 t_p^2}{1 + C^2}\right]. \tag{4.8}$$

With the initial shape of Eq. (4.7) and (4.8), the normalized pulse intensity profile can be determined from Eqs. (4.1) and (4.2). The resulting pulse evolution is exhibited in Figures 4.1 and 4.2 as a function of dimensionless time, $T = \gamma_{eff}\tau$, and dimensionless propagation distance, $Z = \alpha\zeta$ for two values of the chirp. It is seen in the figures that the chirped pulse reshapes faster than does the chirp-free one, quickly burning a "hole" at the center of its intensity profile. This situation is schematically illustrated in Figure 4.3 where the absorption spectrum is displayed as well. The chirped pulse also quickly develops wings in the tails. The drastic reshaping of chirped pulses is due to the initial pulse phase modulation. The latter manifests–in the spectral domain–in

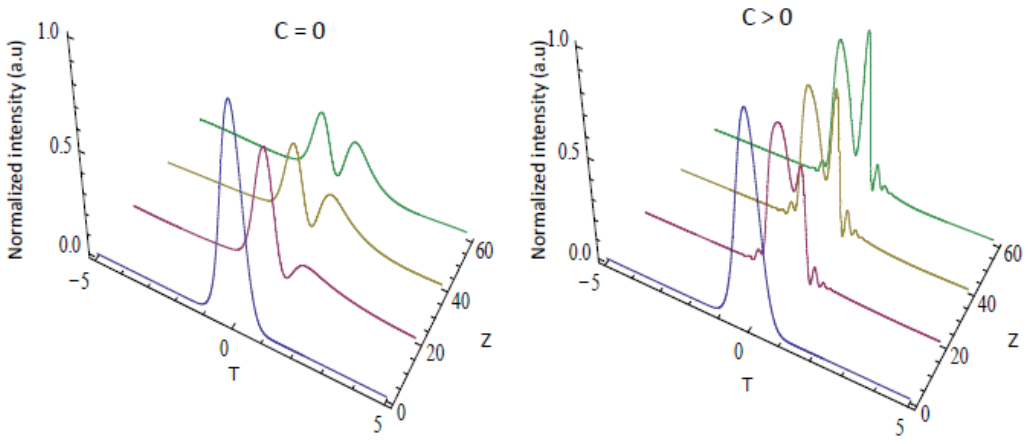

Figure 4.1: Normalized intensity $|\mathcal{E}(T,Z)|^2$ in arbitrary units of a chirped Gaussian pulse as a function of T for several values of Z for C=0 and for $C = 5$.

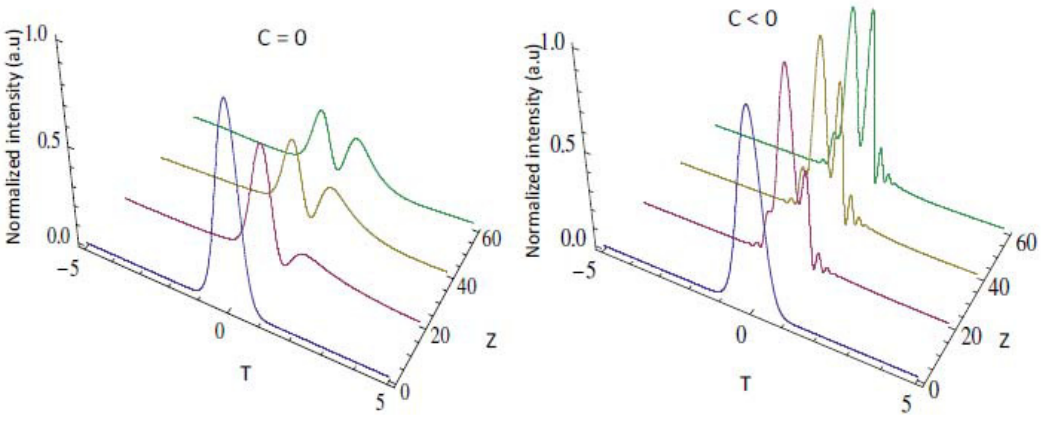

Figure 4.2: Normalized intensity $|\mathcal{E}(T,Z)|^2$ in arbitrary units of a chirped Gaussian pulse as a function of T for several values of Z for C=0 and for $C = -5$.

a broader initial spectrum of the chirped pulse as compared to the chirp-free one. The broader initial spectrum of the chirped pulse causes accelerated spectral broadening and spectral hole burning. As the spectral hole is burnt, the energy of the pulse is

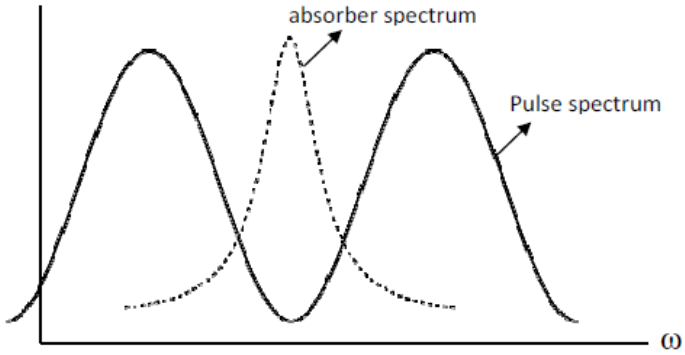

Figure 4.3: The spectrum of absorber medium and chirped short pulse.

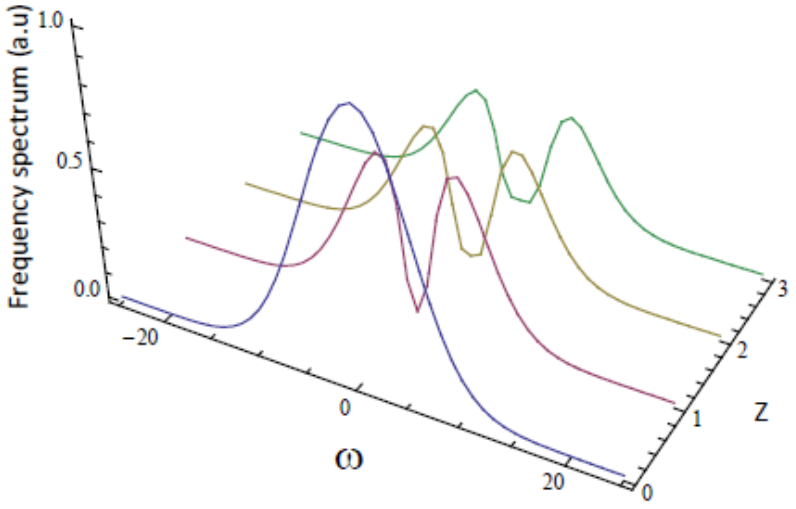

Figure 4.4: Chirped pulse spectrum in arbitrary units as a function of the propagation distance Z for $C = 5$.

pushed away toward the pulse wings, well outside the medium absorption spectrum. As a result, the pulse experiences anomalously low absorption and retains much of its original energy.

To confirm these qualitative conclusions, we numerically calculate and display the

chirped pulse spectrum as a function of the propagation distance in Figure 4.4 where the spectral hole burning is clearly evidenced.

Also, as follows from Eq. (4.8) the initial rms spectral bandwidth of the chirped Gaussian pulse is

$$\Delta\omega \equiv \sqrt{\langle\omega^2\rangle - \langle\omega\rangle^2} = \sqrt{1+C^2}/t_p, \tag{4.9}$$

where the averaging of any function $f(\omega)$ is defined as

$$\langle f(\omega)\rangle = \frac{\int_{-\infty}^{\infty} d\omega\, f(\omega)|\tilde{\mathcal{E}}(\omega)|^2}{\int_{-\infty}^{\infty} d\omega\, |\tilde{\mathcal{E}}(\omega)|^2}. \tag{4.10}$$

To confirm that the spectral rms width of a chirped Gaussian pulse is always greater than its chirp-free counterpart, we worked out in Appendix A, the long-distance asymptotic expression for $\Delta\omega$ as

$$\Delta\omega_\infty(Z) \simeq \sqrt{\frac{1+C^2}{t_p^2} + \frac{\sqrt{2Z(1+C^2)}}{t_p t_{eff}}}, \tag{4.11}$$

where $t_{eff} = \gamma_{eff}^{-1}$ is an effective damping time. It follows from Eq. (4.11) that the

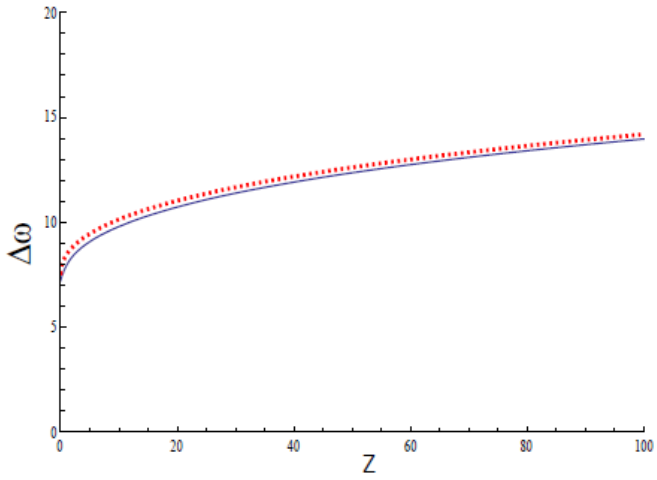

Figure 4.5: The analytical and numerical rms spectral bandwidth of a chirped Gaussian pulse for $C = 5$. The analytical spectra is shown as the dotted line.

bandwidth of Gaussian pulse slowly grows with the propagation distance as $Z^{1/4}$; however, at any propagation distance the chirped pulse spectrum is broader and

it grows faster than the chirp-free pulse spectrum. The analytical result (4.11) is confirmed with numerical simulations in Figure4.5.

As mentioned before, chirped Gaussian pulse propagation in resonant absorbers is accompanied by anomalously low energy losses. The energy losses of chirped pulses are determined by the attenuation factor

$$\Gamma(Z) = \frac{\int_{-\infty}^{\infty} dT \, |\mathcal{E}(T,Z)|^2}{\int_{-\infty}^{\infty} dT \, |\mathcal{E}(T,0)|^2} \tag{4.12}$$

In Appendix B, we analytically determined the asymptotic behavior of the previously introduced, attenuation factor $\Gamma(Z)$ for large Z. It can be expressed as

$$\Gamma_{\infty}(Z) \simeq \exp\left(-\frac{2t_p}{t_{eff}}\sqrt{\frac{2Z}{1+C^2}}\right). \tag{4.13}$$

It follows from Eq. (4.13) that the presence of initial chirp should indeed dramatically reduce energy losses. This conclusion is confirmed by numerical simulations in Figure

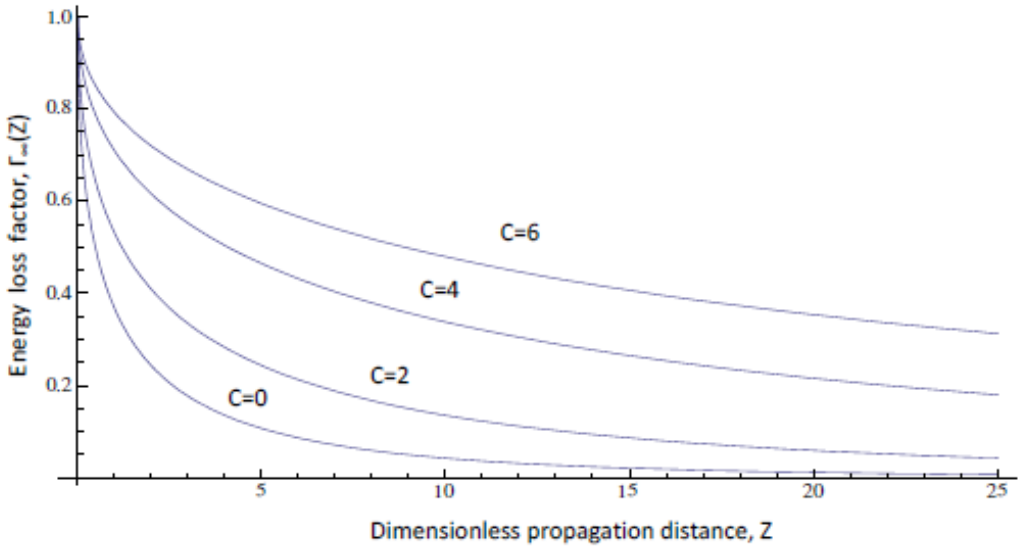

Figure 4.6: Energy loss factor of chirped Gaussian pulse as a function of Z for several values of the chirp parameter.

4.6 where we exhibit the attenuation factor for Gaussian pulses as a function of propagation distance for several values of initial chirp. It is seen in the figure that, for instance, at $Z = 5$, the propagation distance corresponding to 5 typical absorption

lengths, the chirped pulse with C=6 still carries over 60% of its energy while the chirp-free pulse keeps just about 10% of its energy.

From Eq. (2.83) we obtain the profile for long pulse as

$$\mathcal{E}(t,z) = e^{-\alpha z/2} e^{i\beta z/2} \mathcal{E}_0(t - z/c). \tag{4.14}$$

Transforming to dimensionless variables T and Z, we can derive the pulse energy at distance Z from the source as

$$W(Z) \propto \int_{-\infty}^{\infty} dT \left|\tilde{\mathcal{E}}(T,Z)\right|^2 = W(0)e^{-Z} \tag{4.15}$$

The attenuation factor of a long pulse is then given by the expression below

$$\Gamma_0(Z) = e^{-Z}, \tag{4.16}$$

A comparison of the energy loss factor of a short chirped Gaussian pulse and long

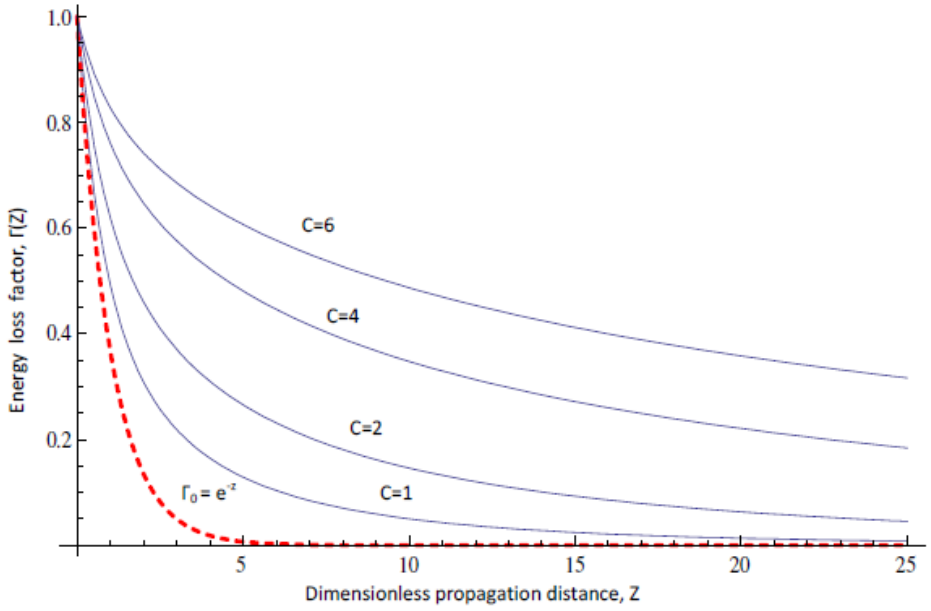

Figure 4.7: Energy loss factor of chirped Gaussian pulse as a function of Z for several values of the chirp parameter and energy loss factor of long pulse e^{-z}.

pulse is made with the help of Figure 4.7.

We can clearly see that chirped Gaussian pulses sustain less energy losses than long pulses. This is due to the fact that short pulses have a very broad energy spectra, which enables them to store a lot of energy in their spectral tails, which an unaffected by the much more narrow loss spectrum of the medium. Conversely, the narrow spectra of long pulses means most of their energy is stored around the center of the pulse, which falls into the narrow spectrum of the absorbing medium, leading to more energy loss through absorption.

4.2.2 Hyperbolic-Secant Pulses

We now consider hyperbolic-secant pulses, briefly discussed in Chap. 3, which arise in the context of soliton fiber lasers and some mode-locked lasers. The field profile of a chirped pulse is given by the expression [48]

$$\mathcal{E}(0,t) = \text{sech}\left(\frac{t}{t_p}\right) \exp\left(-\frac{iCt^2}{2t_p^2}\right). \tag{4.17}$$

Although the previously derived analytical results cannot be easily extended to this case, the behavior of chirped hyperbolic-secant pulses in resonant absorbers can be studied numerically.

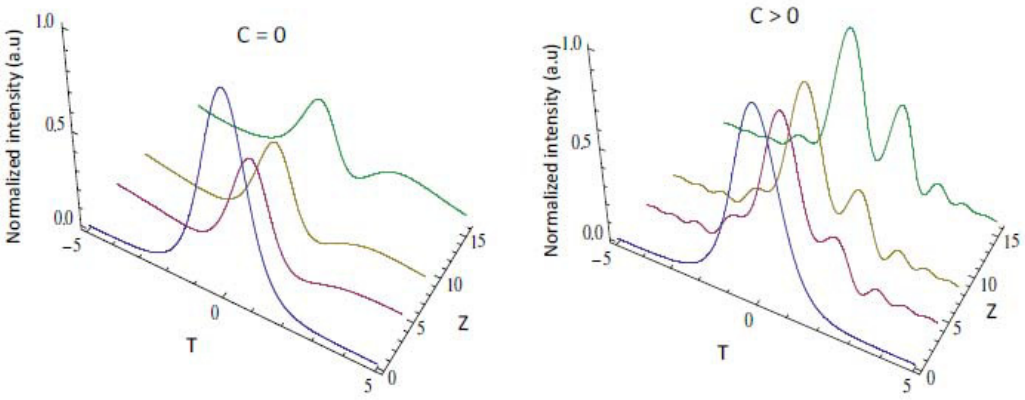

Figure 4.8: Normalized intensity $|\mathcal{E}(T,Z)|^2$ in arbitrary units of chirped secant pulse as a function of T for several values of Z for C=0 and for $C = 2$.

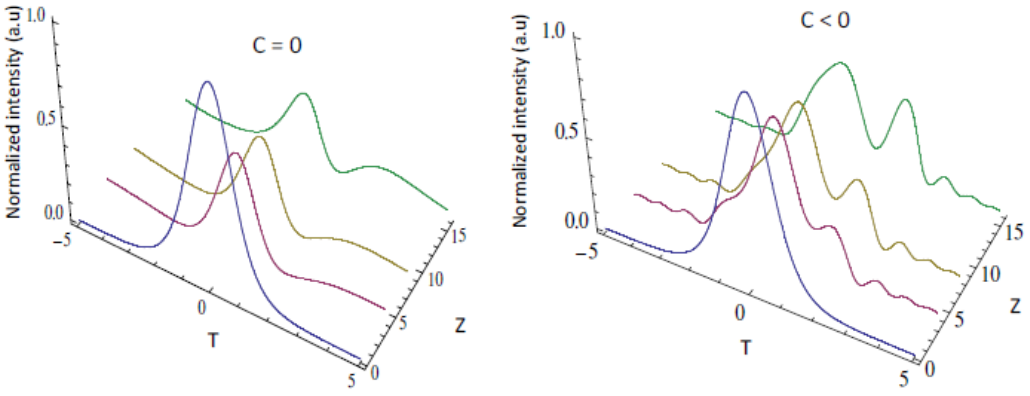

Figure 4.9: Normalized intensity $|\mathcal{E}(T,Z)|^2$ in arbitrary units of chirped secant pulse as a function of T for several values of Z for C=0 and for $C=-2$.

In Figures 4.8 and 4.9 we present the pulse profile evolution for the chirped and chirp-free secant pulses. In Figure 4.8 the chirp is positive, while it is negative in Figure 4.9. It is seen in the figures that the pulse profile reshaping is affected by the sign of the chirp. Further, we display in Figure 4.10 the pulse energy loss factor of secant pulse

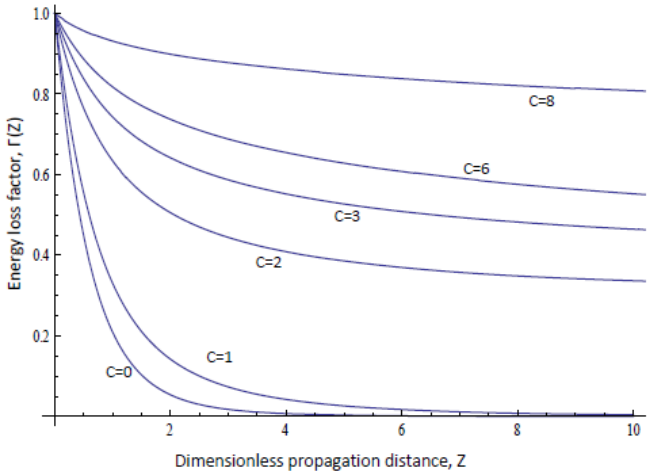

Figure 4.10: Energy loss factor of chirped secant pulse as function of Z for several values of the chirp.

as a function of Z for several values of the chirp.

We can conclude by comparing Figures 4.6 and 4.10 that the chirp dependence of the energy loss suppression is more pronounced for secant than Gaussian pulses.

In this chapter we propose a technique for pulse shaping by using chirped pulses in homogeneously and inhomogeneously broadened linear resonant absorbers. Chirped pulses can be obtained by using a time lens. The time lens is implemented by using an electro-optics phase modulator that can produce quadratic phase modulation [49, 50]. In this study, we first apply chirp to the initial profile of the pulse. This chirped pulse is transmitted through a coherent linear absorbing medium; the pulse quickly burns a "hole" at the center of the intensity profile on propagation in the medium. The incident pulse progressively reshapes on propagation. Chirp free pulses can also reshap when they propagate through absorbers, although from our simulation results it is clear that the pulse shaping is especially pronounced when the pulses are chirped. Since we need to maintain a relatively large propagation distance for the proposed technique to be efficient, we propose to utilize hollow core photonic crystal fibres (HCPCF) filled with a dilute atomic vapour as linear resonant absorbers [51]. In the literature, we find that the absorption lengths of dilute atomic vapours such as potassium (K), rubidium (Rb) and sodium (Na) used in experiments were 1.2 mm [53], 3 cm [52], 30 cm [54] respectively. In our case, the propagation distance as large as $Z = 25$ can be required. We then estimate the required length of HCPCFs to be 7.5m. Each HCPCF, has a hollow core which is surrounded by micro structure

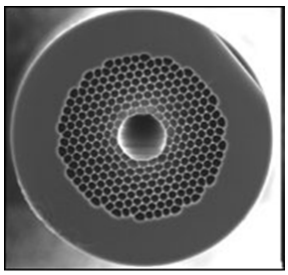

Figure 4.11: Hollow core photonic crystal fiber with a core of 20 μm diameter [55].

cladding. A hollow core is fabricated with a periodic arrangement of air holes in silica. Figure 4.11 shows the HCPCF with a core in 20 μm diameter . A single-mode HCPCFs can arrest the diffraction. HCPCFs also exhibit negligible nonlinear effects on the core and their dispersion can be tuned to zero at a particular wavelength. We assume that we can eliminate fiber GVD at the frequency close to resonance with an atomic transition of neutral gas filling the core of the HCPCF.

Pulses entering the resonant absorbers also create wings in their tails when they

propagate, and at the same time they push all energy towards the pulse wings. For this reason the pulse suffers anomalously low absorption in resonant absorbers. In our technique prechirped pulse enters the medium; the initial chirp can dramatically reduce the energy loss when it propagates through the medium. Highly chirped pulses contain more energy than low chirped pulses after they have traveled over a sufficiently long propagation distance. Shaping of the pulse is also dependent on the sign of chirp parameter in the case of hyperbolic secant pulses.

In this new technique we examined only two common shapes of pulse (Gaussian and secant) which are often used in applications. From the description of pulse compression technique reviewed in chapter 1 we observed that it is a two-step process whereas our technique is a one-step process. In our process, there is no nonlinear effect on the pulses when they propagate whereas most of the pulse shaping process depends on nonlinearity of media.

Most of the techniques of pulse shaping in femtosecond and picosecond regime are implemented by using grating mask where frequency components of pulse spatially disperse, then modulated by spatial light amplitude and phase modulation. In pulse shaping, by spatial filtering, shaping of pulse is mostly dependant on the fabrication of mask. In our case, pulse shaping occurs by the absorbing medium when chirped pulse propagates through it.

Chapter 5

Conclusion

This chapter will summarize the findings of this thesis and provide suggestions for future investigations.

5.1 Conclusions

In this thesis, we have investigated ultrashort pulse propagation in linear absorbing medium in a resonant regime. In this regime the pulse carrier frequency lies in a vicinity of an internal optical resonance of the media. A detailed literature review has been performed on the general theory of pulse propagation in linear absorber medium. Elaborate discussions on various types of chirped pulses were also presented, along with analytical equations to describe the theory properly.

A new technique of pulse shaping is demonstrated in this thesis. Modified and sophisticated pulse shapes can be generated by using the new technique. The influence of initial frequency chirp of the pulse on its subsequent reshaping is also explored in homogeneously and inhomogeneously broadened resonant linear absorbers.

The normalized pulse intensity profiles of commonly used Gaussian and secant pulses were determined by using the fast Fourier method to solve the pulse evolution equations at various propagation distances inside the medium.

To analyze the pulse shaping of pulses with chirp, numerical calculations were also performed for chirped Gaussian pulse spectrum as a function of the propagation distance. The numerical and analytical solutions of the rms spectral bandwidth confirm that the spectral width of a chirped Gaussian pulse is greater than that of a chirp-free pulse.

Although the analytical evaluation of a chirped pulse is more complicated for secant

hyperbolic pulses, we studied the behavior of this pulse by numerical simulation. From the intensity profile, it is evident that chirped pulses are reshaped faster than chirp-free pulses, and that reshaping Gaussian pulses does not depend on the sign of the chirp parameter. Conversely, secant pulses are affected by the sign of chirp.

We also evoluated the loss factor of Gaussian and secant hyperbolic pulses for different values of chirp, especially for short pulses. The attenuation factor of a short pulse (i.e., with a pulse duration much less than that of the relaxation time) was calculated analytically for a chirped Gaussian pulse and confirmed with a numerical result. For very short pulses, the chirp parameter can dramatically reduce the loss factor for the pulse propagating in resonant absorbers. After comparing the chirp dependence of the energy loss factor for Gaussian and secant pulses, we concluded that the effect of chirp is comparably pronounced for secant pulses.

In summary, the novel technique proposed in this thesis is pulse shaping by transmitting prechirped pulses through coherent linear absorbing media. In this process, chirped pulse is allowed to propagate in a linear absorbing resonant media e.g. hollow core photonic crystal fibers filled with a dilute atomic vapor. Inside the media pulse quickly burns a 'hole' in the center of the intensity profile and becomes reshaped with increasing propagation distance. This technique by using chirped pulse resulted in reshaped pulses with low energy losses.

5.2 Future Work

As the numerical simulation results of this thesis were productive, we are encouraged to suggest further theoretical research and experimental demonstration on chirped pulses with different shapes. The solutions of chirped pulses in an amplifying linear resonant medium also need to be investigated in the case of homogeneously and inhomogeneously broadeneding.

Based on our simulation results, we believe that the pulse-shaping techniques of very short pulses discovered in this thesis can be verified and experimentally demonstrated in the future.

Bibliography

[1] S. L. Shapiro, *Ultrashort light pulses: picosecond techniques and applications.* Berlin, Germany: Springer-Verlag, 1977.

[2] J. R. Klauder, A. C, Price, S. Darlington and W. J. Albersheim,"The Theory and Design of Chirp Radars," *Bell System Technical Journal*, vol. 39, pp. 745, 1960.

[3] K. Senthilnathan, L. Qian, P. K. A. Wai and K. Nakkeeran, "Chirped Self-similar Pulse Propagation in Cubic-quintic Media," *PIERS Online*, vol. 3, no. 4, pp. 531-538, 2007.

[4] J. C. Diels, "Femtosecond dye lasers," in *Dye Laser Principles,* F. J. Duarte and L. W. Hillman (Eds.), New York, Academic Press, 1990, Chapter 3.

[5] D. Marcuse, " Pulse distortion in single-mode fibers. 3: Chiped pulses," *Applied Optics*, vol. 20, pp. 3571, 1981.

[6] M. Haner and W. S. Warren,"Generation of arbitrarily shaped pico second optical pulses using an integrated electro optic waveguide modulator," *Applied Optices*, vol. 26, no. 17, pp. 3687, Sep. 1987.

[7] The Free Encyclopedia. [online].
Available: http://en.wikipedia.org/wiki/Femtosecond_pulse_shaping [Accessed:17 Jun. 2011].

[8] The Free Encyclopedia. [online].
Available: http://www1.chem.leeds.ac.uk/PICNIC/members/amplitude1.htm [Accessed:11 Sep. 2010].

[9] A. M. Weinera,"Femtosecond pulse shaping using spatial light modulators," *Review of Scientific Instrument*, vol. 71, no. 5, pp. 1929-1960, May 2000.

[10] D. E. Leaird and A. M. Weiner,"Femtosecond direct space-to-time pulse shaping," *IEEE journal of quantum electronics*, vol. 37, no. 4, pp. 494 - 504, Apr. 2001.

[11] A. Laubereau " External frequency modulation and compression of ps pulses," *Physics Letters*, vol. 29A, pp. 539-540, 1969.

[12] C. E. Cook, "Pulse compression-key to more efficient radar transmission," *Processing of the international radio engineers*, vol. 48, pp. 310-320, 1960.

[13] E. B. Treacy, " Optical pulse compression with diffraction gratings," *IEEE Journal of Quantum Electronics*, vol. 5, pp. 454-460, 1969.

[14] E. B. Traecy, " Compression of picosecond light pulses," *Physics Letters*,vol. 28A, pp. 34-38, 1969.

[15] T. K. Gustafson, J. P. Taran, H. A. Haus, J. R. Lifsitz, and P. L. Kelley, " Self-modulation, selfsteepening, and spectral development of light in small-scale trapped filaments," *Physical Review*, vol. 177, pp. 306-313, 1969.

[16] D. Grischkowsky, "Optical pulse compression," *Applied Physices Letters*, vol. 25, pp. 566, 1974.

[17] J. A. Giordmaine, M. A. Duguay, and J. W. Hansen, "Compression of optical pulses," *IEEE Journal of Quantum Electron*, vol. 4, pp. 252-255, 1968.

[18] J. Diels and W. Rudolph *Ultrashort laser pulse phenomena : Fundamentals, techniques, and applications on a femtosecond time scale.* Academic Press, Second edition, 2006.

[19] C. Froehly, B. Colombeau, and M. Vampouille, " Shaping and analysis of picoseconds light pulses," *Progress in Optics*, vol. 20, pp. 65-153, 1983.

[20] J. P. Heritage, A. M. Weiner, and R. N. Thurston, "Picosecond pulse shaping by spectral phase and amplitude manipulation," *Optics Letter*, vol. 10, no. 12, pp. 609-611, 1985.

[21] A. M. Weiner and J. P. Heritage, "Picosecond and femtosecond Fourier pulse shape synthesis," *Revue Phys. Appl.* , vol. 22, pp. 1619-1628, 1987.

[22] A. M. Weiner, J. P. Heritage, and J. A. Salehi, "Encoding and decoding of femtosecond pulses," *Optices Letters*, vol. 13, no. 4, pp. 300-302, Apr. 1988.

[23] O. E. Martinez, "3000 times grating compressor with positive group velocity dispersion: application to fiber compensation in the 1.3-1.6 ?m region," *IEEE J. Quantum Electron*, vol. 23, pp. 59-64, 1987.

[24] S. Backus, C. G. Durfee III, M. M. Murnane, and H. C. Kapteyn, "High power ultrafast lasers," *Review of Science Instruments*, vol. 69, no. 3, pp. 1207-1223, Mar. 1998.

[25] P. Maine, D. Strickland, P. Bado, M. Pessot, and G. Mourou,"Generation of ultrahigh peak power pulses by chirped pulse amplification," *IEEE Journal of Quantum Electron*, vol. 24, pp. 398-403, Feb. 1988.

[26] D. Marcuse," Pulse distortion in single-mode fibers. Part 2," *Applied Optics*, vol. 20, no. 17, pp. 2969-2974, 1981.

[27] M. Born and E. Wolf, *Principles of optics: Electromagnetic theory of propagation, interference and diffraction of light.* Oxford, Pergaman Press, 1975, fifth edition.

[28] L. Allen and J. H. Eberly, *Optical Resonance and Two-Level Atoms.* Dover: New York, 1987.

[29] M. J. Lighthill,"Group velocity," *IMA J Appl Math*, vol. 1, no. 1, pp. 1-28, 1965.

[30] L. Brillouin, *Wave propagation and group velocity.* New York, Academic Press, 1960.

[31] L. A. Vainshtein, "Propagation of pulses," *Sov. Phys. Usp.*, vol. 19, pp. 189-205, 1976.

[32] A. Sommerfeld, *Optics.* New York, Academic Press, 1954.

[33] J. D. Jackson, *Classical Electrodynamics.* New York, Wiley, 1962.

[34] H. A. Lorentz, *The Theory of Electrons.* New York, Dover, 1952, Chapter 4.

[35] H.A. Kramers, "Estratto dagli Atti del Congresso," *ternazionale de Fisici Como*, vol. 2, pp. 545, 1927.

[36] R. de L. Kronig, "On the Theory of Dispersion of X-rays," *J. Opt. Soc. Am.*, vol. 12, no. 6, pp. 547-556, 1926.

[37] W. T. Silfvast, *Laser fundamentals.* United States ofAmerica, Cambridge University Press, 1996.

[38] Bruker-Biospin. [online]
Available: http://www.bruker-biospin.com/cwendor.html [Accessed:1 May. 2011].

[39] D. Marcuse," Pulse distortion in single-mode fibers," *Applied Optics*, vol. 19, no. 10, pp. 1653-1660, 1980.

[40] RP Photonics. [online].
Available: http://www.rp-photonics.com/chirp.html [Accessed:25 Jan. 2011].

[41] D. Grischkowsky and A. C. Balant, " Optical pulse compression based on enhanced frequency chirping," *Appllied physics letters*, vol. 41, no. 1, pp. 1-3,Jul. 1982.

[42] A. W. Doerry, " Generating Nonlinear FM Chirp Waveforms for Radar," Sandia National Laboratories, Albuquerque, New Mexico, Sandia Report, 2006.

[43] H. Shen, W. Zhang, X. An and K. S. Kwak," DS-PAM UWB System Using Non-linear Chirp Waveform," *ETRI Journal*, vol. 29, no. 3, pp. 322-328, Jun. 2007.

[44] S. E. Anthony, *Lasers.* United States of America, University Science Books, 1986.

[45] B. A. Malomed and A. Berntso, "Propagation of an optical pulse in a fiber link with random-dispersion management," *Journal of optical society of America B*, vol. 18, no. 9, pp. 1243-1251, 2001.

[46] J. Mrtensson, A. Berntson, M. Westlund, A. Danielsson, P. Johannisson, D. Anderson and M. Lisak,"Timing jitter owing to intrachannel pulse interactions in dispersion-managed transmission system," *Optics Letters*, vol. 26, no. 2, pp. 55-57, Jan. 2001.

[47] C. Rullire, *Femtosecond laser pulses: principles and experiments.* Springer, 2005.

[48] G. P. Agrawal, *Nonlinear Fiber Optics.* San Diego, CA, 2nd edition, Academic Press, 1995, Chap. 3, pp. 63-86.

[49] A. M. Weiner, *Ultrafast optics.* United States of America, John Wiley and Sons, 2009.

[50] P. W. Hawkes, *Advances in Imaging and Electron Physics.* vol. 158, ebook.

[51] P. St. J. Russell,"Photonic Crystal Fibers," *Journal of Lightwave Technology*, vol. 24, no. 12, pp. 4729-4749, Dec. 2006.

[52] P. A. Bokhan and P. Artemovich , *Laser isotope separation in atomic vapour.* Willy-VCH, 2007.

[53] A.Sa, U. Vogl and M. Weitz,"Laser cooling of a potassium-argon gas mixture using collisional redistribution of radiation," *Applied Physics B*, vol. 102, no. 3, pp. 503-507, 2011.

[54] J. Kuhl and G. Marowsk, "Narrow - band dye laser as a light source for fluorescence analysis in the subnanogram range," *Optics Communications*, vol. 4, no. 2, pp. 125-128, Oct. 1971.

[55] Philip Russell,"Photonic Crystal Fiber: Finding the Holey Grail," 2011. [online]. Available: http://www.osa-opn.org/Archives/0707/Features/Feature2.aspx [Accessed: 14 Oct. 2011]

[56] J. D. Murry and J.D. Marry, *Asymptotic Analysis.* Applied Mathematical Sciences, New York: Springer, 1984.

Appendix A: RMS width and spectral spread of chirped Gaussian pulses

RMS width and spectral spread of chirped Gaussian pulses in resonant absorbers in the long propagation distance limit

In this section the analytical calculation RMS width and spectral spread of Gaussian pulse is presented. A chirped Gaussian field pulse in the source plan $z = 0$,

$$\mathcal{E}(t,0) \propto \exp\left[-\tfrac{(1+iC)t^2}{2t_p^2}\right].$$

The spectral amplitude of the pulse is given by

$$\tilde{\mathcal{E}}(\omega,0) \propto \exp\left[-\tfrac{\omega^2 t_p^2}{1+C^2}\right] \exp\left[\tfrac{iC\omega^2 t_p^2}{1+C^2}\right],$$

and the pulse spectrum at propagation distance z is

$$\tilde{\mathcal{E}}(\omega,z) = \tilde{\mathcal{E}}(\omega,0)\exp\left[-\tfrac{2\alpha z}{1+\omega^2 t_{eff}^2}\right].$$

The RMS spectral bandwidth of the chirped pulse is

$$\Delta\omega \equiv \sqrt{\langle\omega^2\rangle - \langle\omega\rangle^2}$$

The averaging of the function is defined by

$$\langle\omega^2\rangle = \tfrac{\int_{-\infty}^{\infty} d\omega\, \omega^2 |\tilde{\mathcal{E}}(\omega)|^2}{\int_{-\infty}^{\infty} d\omega\, |\tilde{\mathcal{E}}(\omega)|^2}.$$

So,

$$\langle\omega^2\rangle = \frac{\int_{-\infty}^{\infty} d\omega\, \omega^2 \exp\left[-\frac{\omega^2 t_p^2}{1+C^2}\right] \exp\left[-\frac{2\alpha z}{1+\omega^2 t_{eff}^2}\right]}{\int_{-\infty}^{\infty} d\omega\, \exp\left[-\frac{\omega^2 t_p^2}{1+C^2}\right] \exp\left[-\frac{2\alpha z}{1+\omega^2 t_{eff}^2}\right]}$$

$$\langle\omega^2\rangle = -(1+C^2)\tfrac{\partial}{\partial t_p^2} \ln \int_{-\infty}^{\infty} d\omega \exp\left[-\tfrac{\omega^2 t_p^2}{1+C^2}\right] \exp\left[-\tfrac{2\alpha z}{1+\omega^2 t_{eff}^2}\right]$$

Let,

$$j(t_p) = \int_{-\infty}^{\infty} d\omega \exp\left[-\tfrac{\omega^2 t_p^2}{1+C^2}\right] \exp\left[-\tfrac{2\alpha z}{1+\omega^2 t_{eff}^2}\right]$$

After introducing the dimensionless variable $Z = \alpha z$,

$$j(t_p) = \int_{-\infty}^{\infty} d\omega \exp\left\{-Z\left[\tfrac{\omega^2 t_p^2}{(Z(1+C^2))} - \tfrac{2}{1+\omega^2 t_{eff}^2}\right]\right\}$$

We will use Laplace method for asymptotic evaluation of integrals which is briefly summarized

Consider an integral

$I = \int_{-\infty}^{\infty} dx \exp\left[-\lambda f(x)\right],$

where $f(x)$ is an arbitrary real function in the limit of very large λ. Expand the function in Taylor series up to the second order

$f(x) \simeq f(x_0) + \frac{1}{2!} f''(x_0)(x - x_0)^2.$

Here at x_0

$$f'(x_0) = 0, \qquad f''(x_0) > 0$$

The integral I is then

$I \simeq \int_{-\infty}^{\infty} dx \exp\left[-\lambda f''(x_0) s^2/2\right],$

where,the variable $s = x - x_0$.

After solving result of the integral is

$I \simeq \sqrt{\frac{2\pi}{\lambda f''(x_0)}} \exp\left[-\lambda f(x_0)\right]$

In the case of multiple minima x_k, the resultant integral is

$I \simeq \sum_k \sqrt{\frac{2\pi}{\lambda f''(x_k)}} \exp\left[-\lambda f(x_k)\right]$

For a more detailed discussion see Ref. [56]

Returning to our case we consider

$j(t_p) = \int_{-\infty}^{\infty} d\omega \exp\left[-Z f(\omega)\right], \qquad Z \gg 1$

where,

$f(\omega) = \frac{\omega^2 t_p^2}{Z(1+C^2)} - \frac{2}{1+\omega^2 t_{eff}^2},$

and

$f'(\omega) = \frac{2\omega t_p^2}{Z(1+C^2)} - \frac{4\omega t_{eff}^2}{(1+\omega^2 t_{eff}^2)^2}$

Setting $f'(\omega) = 0$ to solve for roots,

We have

$2\omega t_p^2(1 + 2\omega^2 t_{eff}^2 + \omega^4 t_{eff}^4) - 4 t_{eff}^2 \omega z(1 + C^2) = 0$

$2\omega \frac{t_p^2}{t_{eff}^2} \frac{1}{t_e^2 ff} + 4\omega^3 (\frac{t_p}{t_{eff}})^2 + \omega^5 t_p^2) - 4\frac{\omega z(1+C^2)}{teff^2} = 0$

For short Gaussian pulse $t_p << t_{eff}$,

$2\omega\left[\omega^4 t_p^2 - \frac{2Z(1+C^2)}{t_{eff}^2}\right] = 0$

Solving gives the roots

$$\omega = 0, \qquad \omega_{1,2} = \pm\left[\frac{\sqrt{2Z(1+C^2)}}{t_p t_{eff}}\right]^{1/2}, \qquad \omega_{3,4} = \pm i\left[\frac{\sqrt{2Z(1+C^2)}}{t_p t_{eff}}\right]^{1/2}.$$

Root ω_3 and ω_4 is unphysical because ω must be real.

Now,

$f''(\omega) = \frac{2t_p^2}{Z(1+C^2)} - 4t_{eff}^2\left[\frac{1}{(1+\omega^2 t_{eff}^2)^2} - \frac{2\omega(2\omega t_{eff}^2)}{(1+\omega^2 t_{eff}^2)^3}\right]$

Evaluating $f''(\omega)$ at the roots

$f''(0) = 2\frac{2t_p^2}{Z(1+C^2)} - 4t_{eff}^2 \simeq -4t_{eff}^2$

This root is unphysical because $f''(0) < 0$

$$f''\left(\pm\left[\frac{\sqrt{2Z(1+C^2)}}{t_p t_{eff}}\right]^{1/2}\right) = \frac{2t_p^2}{Z(1+C^2)} - 4t_{eff}^2\left[\frac{1}{\left(1+\frac{\sqrt{2Z(1+C^2)}t_{eff}}{t_p}\right)^2} - \frac{4\sqrt{2Z(1+C^2)}\frac{t_{eff}}{t_p}}{\left(1+\frac{\sqrt{2Z(1+C^2)}t_{eff}}{t_p}\right)^3}\right]$$

$$\approx \frac{2t_p^2}{Z(1+C^2)} - 4t_{eff}^2\left[\frac{1}{\left(\frac{\sqrt{2Z(1+C^2)}t_{eff}}{t_p}\right)^2} - \frac{4}{\left(\frac{\sqrt{2Z(1+cC2)}t_p}{t_{eff}}\right)^2}\right], \qquad \frac{t_{eff}}{t_p} \gg 1$$

$$= \frac{8t_p^2}{Z(1+C^2)}$$

And

$$f\left(\pm\left[\frac{\sqrt{2Z(1+C^2)}}{t_p t_{eff}}\right]^{1/2}\right) = \frac{t_p\sqrt{2Z(1+C^2)}}{t_{eff}Z(1+C^2)} + \frac{2}{\left(1+\frac{\sqrt{2Z(1+C^2)}t_{eff}}{t_p}\right)}$$

$$\approx \frac{t_p}{t_{eff}}\frac{\sqrt{2Z(1+C^2)}}{Z(1+C^2)} + \frac{2}{\sqrt{2Z(1+C^2)}\frac{t_{eff}}{t_p}}$$

$$= 2\frac{t_p}{t_{eff}}\frac{\sqrt{2Z(1+C^2)}}{Z(1+C^2)}$$

So,

$$Zf(\pm\left[\frac{\sqrt{2Z(1+C^2)}}{t_p t_{eff}}\right]^{1/2}) = 2\frac{t_p}{t_{eff}}\frac{\sqrt{2Z(1+C^2)}}{(1+C^2)}$$

Hence

$j(t_p) = \int_{-\infty}^{\infty} d\omega \exp\left[-Z\frac{\omega^2 t_p^2}{(Z(1+C^2))} - \frac{2}{1+\omega^2 t_{eff}}\right] \approx 2\sqrt{\frac{2\pi}{Zf''(\omega_{1,2})}}\exp(-Zf(\omega_{1,2}))$

$$= 2\sqrt{\frac{2\pi}{\frac{8t_p^2}{(1+C^2)}}}\exp(-2\frac{t_p}{t_{eff}}\frac{\sqrt{2Z(1+C^2)}}{(1+C^2)})$$

$$= 2\sqrt{\frac{\pi(1+C^2)}{4t_p^2}}\exp(-2\frac{t_p}{t_{eff}}\sqrt{\frac{2Z}{(1+C^2)}})$$

Now,

$$\ln j(t_p) = -2\frac{t_p}{t_{eff}}\sqrt{\frac{2Z}{(1+C^2)}} - 1/2\ln t_p^2 + 1/2\ln(\frac{\pi(1+C^2)}{2})$$

Let, $x = t_p^2$

$$\langle\omega^2\rangle = -(1+C^2)\frac{\partial}{\partial x}\left[-2\frac{\sqrt{x}}{t_{eff}}\sqrt{2Z(1+C^2)} - 1/2\ln x\right]$$

$$\langle\omega^2\rangle = (1+C^2)\left[\frac{1}{t_{eff}t_p}\sqrt{\frac{2Z}{(1+C^2)}} + \frac{1}{2t_p^2}\right]$$

$$\langle\Delta\omega^2\rangle = \frac{(1+C^2)}{2t_p^2} + \frac{1}{t_{eff}t_p}\sqrt{\frac{2Z}{(1+C^2)}}$$

Finally the long-distance asymptotic expression for $\Delta\omega$ is

$$\Delta\omega_\infty(Z) \simeq \sqrt{\frac{1+C^2}{2t_p^2} + \frac{\sqrt{2Z(1+C^2)}}{t_p t_{eff}}}.$$

Appendix B: Attenuation factor of chirped Gaussian pulses

Asymptotic expression for attenuation factor of chirped Gaussian pulses in resonant absorbers

In this section the analytical calculation attenuation factor of Gaussian pulse is presented. A chirped Gaussian field pulse in the source plan $z = 0$,

$\mathcal{E}(t,0) \propto \exp\left[-\frac{(1+iC)t^2}{2t_p^2}\right].$

The energy attenuation factor of the pulse is

$\Gamma(z) = W(z)/W(0).$

The pulse energy at any propagation distance within a resonant absorbing medium is determine by the square modulus of the field envelope,

$W(z) \propto \int_{-\infty}^{\infty} dt \left|\mathcal{E}(t,z)\right|^2.$

By using the Fourier transform properties, the energy at any propagation distance z is expressed by

$W(z) = \int_{-\infty}^{\infty} d\omega \left|\tilde{\mathcal{E}}(\omega,0)\right|^2 \exp\left[-\frac{2\alpha z}{(1+\omega^2 t_{eff}^2)}\right].$

and when the propagation distance $Z = 0$, the energy is

$W(0) = \int_{-\infty}^{\infty} d\omega \left|\mathcal{E}(\omega,0)\right|^2.$

The resultant energy attenuation factor,

$\Gamma(z) = \frac{\int_{-\infty}^{\infty} d\omega \left|\tilde{\mathcal{E}}(\omega,0)\right|^2 \exp\left[-\frac{2\alpha z}{(1+\omega^2 t_{eff}^2)}\right]}{\int_{-\infty}^{\infty} d\omega \left|\tilde{\mathcal{E}}(\omega,0)\right|^2}$

Let,

$j(t_p) = \int_{-\infty}^{\infty} d\omega \exp\left[-\frac{\omega^2 t_p^2}{1+C^2}\right] \exp\left[-\frac{2\alpha z}{1+\omega^2 t_{eff}^2}\right]$

Similarly by using the Laplace method for asymptotic evaluation of integrals, we can write from Appendix A

$j(t_p) = 2\sqrt{\frac{\pi(1+C^2)}{4t_p^2}} \exp(-2\frac{t_p}{t_{eff}}\sqrt{\frac{2Z}{(1+C^2)}})$

And

$W(0) = \int_{-\infty}^{\infty} d\omega \left|\tilde{\mathcal{E}}(\omega,0)\right|^2 = \int_{-\infty}^{\infty} d\omega \exp\left[-\frac{\omega^2 t_p^2}{1+C^2}\right]$

$= \sqrt{\frac{\pi(1+C^2)}{t_p^2}}$

The energy attenuation factor for sufficiently large propagation distance

$$\Gamma_\infty(Z) = W(Z)/W(0) \simeq \frac{\sqrt{\frac{\pi(1+C^2)}{t_p^2}}\exp(-2\frac{t_p}{t_{eff}}\sqrt{\frac{2Z}{(1+C^2)}})}{\sqrt{\frac{\pi(1+C^2)}{t_p^2}}}$$

So, the energy attenuation factor of a very short Gaussian pulse in the long propagation distance limit is

$$\Gamma_\infty(Z) \simeq \exp\left(-\frac{2t_p}{t_{eff}}\sqrt{\frac{2Z}{1+C^2}}\right).$$

Appendix C: Mathematica code

The following mathematica code were used for evaluate Intensity of chirped Gaussian pulse:

```
ClearAll["Global‘*"]

Omega[T_, C_] = Exp[-(1 + I*C)*2*T^2];

data1[C_] = Table[Omega[T, C], {T, -5, 5, .01}];

Omega[nu_, C_?NumericQ] := 1/(2*Pi)*Fourier[data1[C]];

s[nu_, z_] = Exp[-z/(1 - I*nu)/2];

data2[z_] = Table[s[nu, z], {v, 0, 2000*Pi, 2*Pi}];

omega[T_, z_, C_?NumericQ] := InverseFourier[data2[z]*omega[nu, C]];

x = Range[-5, 5, .01];

output =
Table[Thread[{x, Abs[omega[T, z, C]]^2/0.0253}], {z, {0, 20, 40,
60}}];

ListLinePlot[output, PlotRange -> All]

to3D[list_, val_] := Insert[#, val, 2] & /@ list

Graphics3D[
Riffle[Take[ColorData[1, "ColorList"], 4],
Line /@ to3D @@@ Thread[{output, {0, 20, 40, 60}}]], Axes -> True,
BoxRatios -> {GoldenRatio, 1, 1}
BoxStyle -> Directive[Dashed, None], Boxed -> False]
```

The code used for find out Pulse spectrum and attenuator factor are given below:

```
ClearAll["Global‘*"]

Omega[T_, C_] = Exp[-(1 + I*C)*2*T^2];
```

```
data[C_] = Table[Omega[T, C], {T, -5, 5, sampling time}];


Omega[nu_, C_?NumericQ] := 1/(2*Pi)*Fourier[data[C]];

output = Table[{nu, (Abs[
omega[nu,C] - 2 z/(1 + (nu)^2)]])^2}, {z, {0, 1, 2,
3}}, {nu, -25, 25}];

ListLinePlot[output, PlotRange -> Full]

to3D[list_, val_] := Insert[#, val, 2] & /@ list

Graphics3D[
Riffle[Take[ColorData[1, "ColorList"], 4],
Line /@ to3D @@@ Thread[{output, {0, 1, 2, 3}}]], Axes -> True,
BoxRatios -> {GoldenRatio, 1, 1}, Boxed -> False]
```